Radiation Effects & Defects in Solids, Vol. 148, pp. 269–318
Reprints available directly from the publisher
Photocopying permitted by license only

CLUSTERING THEORY OF ATOMIC DEFECTS*

NASR M. GHONIEM

University of California at Los Angeles, Los Angeles, CA 90095-1600, USA

(Received 15 December 1997; In final form 4 December 1998)

Clustering of atomic defects leads to changes in the microstructure of materials, and hence induces drastic variations in their properties. In many technical fields, the role of defect clustering is very significant, and is sometimes limiting to further progress. We present here a comprehensive review of the theory of atomic defect clustering under non-equilibrium conditions, particularly encountered during irradiation of materials with energetic particles, as well as during material processing by energetic sources. These conditions are met in a wide range of technical applications, ranging from nuclear and fusion energy to microelectronics and surface engineering. We first present a general stochastic framework for the evolution of atomic clusters, and show how this can be described within the context of death-and-birth processes. This leads to the well-known master equation for microscopic atomic clusters. In the limiting case of a Poissonian process for the transition probabilities between cluster sizes, the master equation tends, in the macroscopic limit, to the mean-field approximation embodied by the theory of rate processes. When atomic clusters grow or shrink by the absorption of single atomic defects, a continuum Fokker–Planck approximation can be derived. Within this approximation, the evolution of interstitial loops, voids, bubbles, and general clusters of complex phases is presented, and in some cases, good agreement with experiments is obtained. It is shown that because of coalescence reactions, the evolution of surface atomic clusters during atom deposition processes is best described by kinetic moment equations, directly derived from rate equations. It is shown that breaking the symmetry of space or time leads to drastic variations in the size and space distributions of defect clusters. Examples are given for pulsed irradiation conditions, where it is shown that non-linear rate processes enhance cluster formation during on-time, and could lead to their dissolution during the off-time at high temperature. On the other hand, fluctuations are shown to result in instabilities and spatial self-organization of defect clusters. Description of pattern formation during irradiation, such as void and interstitial loop lattices, is very well described by a Ginzburg–Landau type equation, reminiscent of phase transitions under thermodynamic equilibrium conditions.

Keywords: Atomic defects; Clusters; Irradiation; Non-equilibrium

---

* *Proceedings of the Kiritani Symposium on Structural Defects in Advanced Materials*, Inuyama, Aichi, Japan, December 18–20, 1996.

1 INTRODUCTION

Clustering of atomic size defects in materials is a process which embodies a rich variety of physical mechanisms, and which has significant implications to a wide range of material technologies. Strong deviations from thermodynamic equilibrium conditions drive defects into agglomeration, as an attempt to reduce the system's free energy. Materials inevitably contain atomic defects, in the form of vacancies, self-interstitials, impurity atoms or insoluble gaseous species. In some situations, these defects are externally introduced into the material. Examples of this can be found in structures under neutron irradiation, or in materials that are processed by ion beams, plasmas or other high-energy sources.

Apart from the valuable insight gained by understanding mechanisms of atomic defect clustering, advancing a multitude of cutting-edge technologies is dependent on finding ways to modify the process of defect agglomeration. Energetic neutrons bombard a number of critical materials in nuclear fission reactors. Materials used as nuclear fuels, structural materials, the pressure vessel as well as instrumentation materials are all subjected to the generation of non-equilibrium concentrations of atomic defects. Energetic neutron collisions with lattice atoms produce intrinsic lattice defects, as well as extrinsic impurities or insoluble gas atoms. Likewise, in a fusion energy system, many materials will be driven out of equilibrium as a result of intense neutron bombardment. Examples are the first wall and blanket structure, plasma interactive components, magnet materials, instrumentation and other special purpose materials. In space and defense technologies, other phenomena take place as a result of the interaction of radiation with materials. For example, computer chips on board of space vehicles and satellites are constantly being bombarded by galactic radiation, producing lattice defects, which can impair their function. Systems, which are built around high energy beam sources (e.g., accelerators, electron beam systems, laser beam systems, etc.), are also under the action of the same conditions that drive materials out of equilibrium. More recently, several material processing technologies take advantage of ion beams, plasma sources or laser beams. Manufacturing of semi-conductor computer chips is a prime example of such material modification techniques. It is now recognized that the limitation on decreasing chip size is determined by the concentration of atomic defects produced during implantation or etching.

In this paper, we review theoretical developments in the treatment of atomic clustering, with applications in two general areas. The first one is the evolution of microstructure under irradiation conditions. The second area of interest is atomic clustering on surfaces during deposition of vapor or energetic atoms. To accomplish this task, we will first start with a stochastic description of atomic clustering. Thus, we introduce the general form of master equations and the corresponding rate theory description. We show that if coalescence mechanisms are taken into account, as in the case of surface atomic clusters, the master equation description is necessary. One solution method, based on moments of these equations, is discussed. In cases where the agglomeration of atomic clusters is primarily a result of simple atom absorption or emission, a very useful approximation is the Fokker–Planck theory. In phase space, we represent the dimensionality of clusters by the number of atomic species involved within. Thus, one-dimensional clustering means that one species is involved. We focus on a coupled approach to nucleation and growth, and look for ways to solve for the evolution of the size distribution in a given phase space. Thus, examples of one-dimensional clustering will be given for interstitial dislocation loop evolution in irradiated materials, and for the evolution of surface atomic clusters during plasma-assisted deposition. In situations where we have helium filled bubbles in solids, we develop methods to determine their evolution in two-dimensional phase space.

The discussion highlighted above is based on a homogeneous space and time state. Some very interesting features take place during atomic clustering if space–time inhomogeneities exist. Pulsed or transient irradiation of materials promotes certain non-linearities in atomic clustering, and leads to drastic variation in the size and density of clusters. On the other hand, spatial fluctuations in defect densities lead to symmetry breaking, and the emergence of self-organized microstructure. We will deal with these two areas in Section 6, followed by conclusion and future outlook in Section 7.

2 GENERAL THEORY OF ATOMIC CLUSTERING

2.1 Birth-and-Death Processes

Under the non-equilibrium conditions that drive atomic defect clustering, the size of each individual cluster grows or shrinks by

a process of accretion or emission. The "step" which changes the cluster size is controlled by fluctuations in the neighborhood of the cluster. Thus, an appropriate framework for these events is the theory of stochastic processes. Defect clusters are either "born" or they "die" with each event. Many physical phenomena have similar characteristics, and are generally described as birth-and-death processes. As indicated earlier, the size of clusters is a main variable, and is randomly distributed in this description. Each size may contain several atomic species.

If the size of the transition step is by single atomic defects, then $\Delta\bar{x} \ll \bar{x}$. Here, $\Delta\bar{x}$ is the step size and $\bar{x}$ is a vector of components representing the cluster constituents. Clustering may occur via multiple atom aggregation, and $\Delta\bar{x}$ is still smaller than $\bar{x}$. Finally, the typical case of coalescence is associated with a transition, where $\Delta\bar{x}$ is of the same order of $\bar{x}$.

In the master equation description, one assigns to the system a set of transition probabilities describing the process of cluster size variation in size space. Consider that the cluster size $\bar{x}$ is discrete, and is represented by a sequence of numbers, each describing the number of a particular specie. Thus, instead of the vector notation, we use an index notation, as follows:

$C_{ijklm...}$ = Fractional concentration of defect clusters containing i defects of type α, j defects of type β, etc. Thus, the fractional concentration of self-interstitial loops is simply denoted by C_i, where i is the number of self-interstitials in the loop. C_{ij} denotes the fractional concentration of helium bubbles, where i represents the number of vacancies and j the number of helium atoms. The notation can be extended to more complex defect phases in the solid. Since $C_{ijklm...}$ is fractional, it is precisely the probability of finding a defect cluster of these constituents.

The transition probabilities, ω, depend on a set of integers $\Delta_{ijk...}$, which may be positive, negative or zero, and they describe the step size $\Delta\bar{x}$. The conditional probability of a transition describing the change of the number $(i,j,k,l,\ldots)$ due to a step $(\Delta_{ijk...})$ is given by

$$\omega(\{(i,j,k,l,\ldots) - \Delta_{ijkl...}\} \rightarrow \{i,j,k,l,\ldots\}). \tag{1}$$

Thus in a time interval Δt, and considering all possible forward and backward transitions, the probability function $C_{ijkl\ldots}$ will change as

$$\Delta C_{ijkl\ldots}(t) = \Delta t \left(\begin{array}{l} \sum_{\Delta} \omega(\{(i,j,k,l,\ldots) - \Delta_{ijkl\ldots}\} \rightarrow \{ijkl\ldots\}) \\ \quad \times C(\{(i,j,k,\ldots) - \Delta_{ijkl\ldots}\}, t) \\ - \sum_{\Delta} \omega(\{i,j,k,\ldots\} \rightarrow \{(i,j,k,\ldots) + \Delta_{ijkl\ldots}\}) C(\{i,j,k,\ldots\}, t) \end{array} \right). \tag{2}$$

The fundamental relationship, represented by (2) is the Smoluchowski–Chapman–Kolmogorov (SCK) equation [1], applied to defect clustering. Taking the limit as $\Delta t \rightarrow 0$, one obtains the master equation, which now describes the birth-and-death process of the cluster. Thus, the most general case of defect clustering can be described by the following master equation:

$$\frac{\mathrm{d}}{\mathrm{d}t} C_{ijkl\ldots}(t) = \left(\begin{array}{l} \sum_{\Delta} \omega(\{(i,j,k,l,\ldots) - \Delta_{ijkl\ldots}\} \rightarrow \{ijkl\ldots\}) \\ \quad \times C(\{(i,j,k,\ldots) - \Delta_{ijkl\ldots}\}, t) \\ - \sum_{\Delta} \omega(\{(i,j,k,\ldots\} \rightarrow \{(i,j,k,\ldots) + \Delta_{ijkl\ldots}\}) C(\{i,j,k,\ldots\}, t) \end{array} \right). \tag{3}$$

It has been shown by Malek-Mansur and Nicolis [2] that if a Poisson distribution describes the transition probabilities ω, their microscopic statistical averages become identical to the macroscopic system averages used in reaction rate theories. Thus, the equilibrium laws of reaction rate theory become exact consequences of the master equation.

Averaging over transition probabilities leads to the popular reaction rate theory, which now discards important aspects of defect fluctuations. These are related to the system size, range over which fluctuations extend, and correlation length over which two parts of the system can feel each other. We will later show that in a system that is macroscopically homogeneous, locally, fluctuations break this homogeneity and lead to

the emergence of spatial defect patterns. As soon as the system deviates from the uniform state described by the spatially averaged rate equations, non-linear couplings between neighboring volume elements take place. As a result, a spatially uniform description of defect concentrations becomes inadequate.

2.2 Stochastic Fluctuations in Defect Fields

The starting point of the theory of microstructure evolution is the SCK equation for a Markovian process [3] presented above. In the continuum limit in size space, summations are replaced by integrals, and we have

$$\frac{\partial C}{\partial t} = \int [\omega(\bar{x}', \bar{x}, t')C(\bar{x}', t') - \omega(\bar{x}, \bar{x}', t)C(\bar{x}, t')]\, \mathrm{d}\bar{x}', \tag{4}$$

where $C(\bar{x}, t)$ is the probability distribution for the stochastic variable $\bar{x}$ at time t. The transition probability per unit time from state $\bar{x}$ to state $\bar{x}'$ at time t is $\omega(\bar{x}, \bar{x}', t)$. Equation (4) can be reduced to a deterministic rate equation for the concentration of a specific defect cluster (e.g., di-interstitials, di-vacancies, tri-vacancies and two helium atoms, etc.), if the transition probabilities, ω, are replaced by average macroscopic reaction rates. This mean-field approximation does not take into account the statistical nature of defect production, cascade effects, and the arrival and absorption of single and multiple defects at defect clusters.

Since defect clustering in irradiated solids is driven by the concentration of three types of monomers (vacancies, interstitials, and helium), we would have a coupled hierarchy of discrete equations for the probability distribution, C, using rate or master equations of the form given by Eq. (4). The transition probability from a defect cluster size $\bar{x}'$ to $\bar{x}$ may be re-defined in the following way:

$$\omega(\bar{x}', \bar{x}, t') \equiv W(\bar{x}', \bar{x} - \bar{x}', t') \equiv W(\bar{x} - \bar{r}, \bar{r}, t, \tau). \tag{5}$$

2.3 The Fokker–Planck Approximation

In certain applications of Markov chains, the spacing between the states is small, and the hierarchy of discrete master equations can be replaced

by an equivalent continuum Fokker–Planck (F–P) equation. It is interesting to note that except for small size interstitial loops, large defect clusters have low mobility inside irradiated solids. On the other hand, when we consider the formation of surface atomic clusters during plasma or ion beam deposition, the mobility of large clusters becomes significant.

In Eq. (5), we distinguish between slow $(\bar{x}, t)$ and fast $(\bar{r} = \bar{x} - \bar{x}', \tau)$ variables. By expanding the function $W(\bar{x} - \bar{r}, \bar{r}, t, \tau)C(\bar{x} - \bar{r}, t)$ in a Taylor series for the slow variable, truncating to second order, and integrating over an appropriate correlation time, T, we obtain the F–P equation

$$\frac{\partial C(\bar{x}, t)}{\partial t} = \frac{1}{2}\sum_{i,j} \frac{\partial^2}{\partial x_i \partial x_j}(\langle r_i r_j \rangle C) - \sum_i \frac{\partial}{\partial x_i}(\langle r_i C \rangle), \tag{6}$$

where

$$\langle r_i(\bar{x}, t) \rangle = \frac{1}{T}\int_0^T \int_1^\infty r_i \omega(\bar{x}, r, t, \tau)\, \mathrm{d}\bar{r}\, \mathrm{d}\tau, \tag{7}$$

and

$$\langle r_i(\bar{x}, t) r_j(\bar{x}, t) \rangle = \frac{1}{T}\int_0^T \int_1^\infty r_i r_j \omega(\bar{x}, \bar{r}, t, \tau)\, \mathrm{d}\bar{r}\, \mathrm{d}\tau. \tag{8}$$

The indices i or j represent the dimension in cluster size space (1-D for interstitial loops and 2-D for He–V clusters). Equations (7) and (8) give the first and second moments of the transition probabilities. The correlation time, T, is chosen to represent the appropriate physics of the relevant transition (e.g., inverse of arrival frequency for single-atom transitions or cascade-production frequency for cascade-induced transitions). Equation (7) represents the elements of a drift vector, while Eq. (8) is used to derive the elements of a dispersion tensor.

The following is a summary of the general procedure for the implementation of the theory. A set of rate equations for the concentrations of single defects and small defect aggregates is formulated to represent time-dependent nucleation. Larger-size defect clusters are treated by the F–P approximation given by Eq. (6), with the transition moments obtained in Eqs. (7) and (8). Rate equations are coupled to the F–P equation through a flux boundary condition, and the solution is obtained semi-analytically as in [4] or numerically as in [5]. We will proceed now with applications of the general theory to various important situations of technical interest.

3 INTERSTITIAL LOOP EVOLUTION UNDER IRRADIATION

When pure materials are irradiated with energetic particles, self-interstitial atoms are produced at the rate of atomic displacements. However, few of these self-interstitials survive immediate recombination within the cascade region, and one must take into account the fraction of surviving defects. Under the conditions of electron or light ion irradiation, however, single interstitial atoms dominate over small clusters produced in collision cascades. In the limit of Poissonian transition rates, master equations can be cast as macroscopic rate equations, and rate constants are obtained.

3.1 Rate Constants

In the *jump* method [6], the reaction between diffusion species proceeds by a surface control mechanism. On the other hand, the rate constants in the *diffusion* method are obtained by solving steady-state diffusion (Eq. (6)). Defining the instability radius of a particular cluster, R, as the radius at which point defects will inevitably be attracted towards the cluster (interaction energy $\approx kT$), then

$$R = Z(r)r, \tag{9}$$

where r is the physical cluster radius and $Z(r)$ is a size-dependent bias factor (capture efficiency). Results of detailed elasticity calculations of Wolfer and Ashkin [7] have been used in Eq. (9). The overall reaction rate constant is obtained in a manner similar to that used to determine the overall heat flux with series resistance [8].

Define x as the cluster size in atomic units, i for an interstitial, v for a vacancy, l for a loop, and c for a cavity. For a spherical cluster in FCC materials, the following impingement frequencies, K (s^{-1}), can be derived [8]:

$$K^{c}_{v,i}(x) = \frac{2.216[Z^{c}_{v,i}(x)]^2 x^{2/3}}{1 + 0.1128 Z^{c}_{v,i}(x) x^{1/3}} \nu_{v,i} \exp\left(\frac{-E^{m}_{v,i}}{kT}\right), \tag{10}$$

where ν is the atomic vibration frequency, $E^{m}_{v,i}$ the vacancy–interstitial migration energy, k the Boltzmann constant, and T the absolute irradiation temperature. For large size cavities the reaction rate is purely

diffusion controlled and the impingement frequency is proportional to $x^{1/3}$. Interstitial clusters are treated as small spherical inclusions with the application of Eq. (2) up to a maximum size $z_i^{\max}$ of few interstitials. However, larger sizes can be considered as two-dimensional disks and the interaction with point defects is only surface controlled. The relevant impingement frequency is then

$$K_{v,i}^{l}(x) = 1.555 Z_{v,i}^{l}(x) x^{1/2} \nu_{v,i} \exp\left(\frac{-E_{v,i}^{m}}{kT}\right). \tag{11}$$

The emission of vacancies from the surface of vacancy clusters is included in this model. However, point defect thermal emission from interstitial loops is not considered because of the small probability of this process for small size loops. The only thermal dissociation process treated is that for di-interstitial break-up. The emission *rate* of vacancies from a vacancy cluster size x is given by

$$\gamma_v^e(x) = K_v^e(x) C_v^e \left[\left(\frac{1.28 g a^2}{kT}\right) x^{-1/3}\right], \tag{12}$$

where a (cm) is the lattice constant, g (eV/cm^2) the surface energy, and C_v^e the thermal matrix fractional vacancy concentration. Di-interstitial and di-vacancy thermal dissociation rates are given as

$$\gamma_{v,i}^{e,i}(2) = K_{v,i}^{e,i}(2) \exp\left(-\frac{E_{2v,2i}^{B}}{kT}\right), \tag{13}$$

where E_{2v}^{B} and E_{2i}^{B} are the binding energies for di-vacancies and di-interstitials, respectively.

3.2 Rate Equations

The basic limitation to the rate theory lies in the one-to-one relationship between the number of simultaneous differential equations and the number of species in a cluster. Computations with individual rate equations representing independent clusters become prohibitively expensive for large sizes (see Refs. [9–17]). The need for correspondence between theory and experiment has prompted the development of approximate

computational methods for the kinetics of defect clustering. Kiritani [9] developed a scheme for nucleation and growth, in which clusters within a range of sizes are grouped together, and has applied the method to vacancy agglomeration after quenching. Hayns [10] applied the Kiritani grouping scheme to study the nucleation and growth of interstitial loops during irradiation.

A different approach to the study of the nucleation and growth of defect clusters has considered solving continuum equations rather than rate equations. Wolfer *et al.* [11] demonstrated that rate equations describing clustering kinetics can be condensed into one Fokker–Planck continuum equation. The latter was interpreted as a diffusion equation with drift terms. They showed that void nucleation and growth could be both incorporated into such a unified formalism. Sprague *et al.* [12] were able to describe vacancy clusters containing up to 3920 vacancies by descretizing a diffusion-type equation with variable diffusivity. Hall [13] investigated point defect agglomeration considering a different form of the continuum description. Only cluster concentrations were expanded in a Taylor series, and the resulting set of rate equations condensed into one partial differential equation.

In developing the theoretical model for interstitial loop evolution, we will follow the rate theory formulation of Ghoniem and Cho [8]. Separate rate equations will be constructed for single vacancies, single interstitials and clusters of up to 4 vacancies and 4 interstitials. Larger size defects, however, are treated by the one-dimensional Fokker–Planck equation for both voids and interstitial loops. The concentrations of single vacancies and vacancy clusters up to tetra-vacancies are governed by

$$\frac{dC_v}{dt} = P_v + K_i^c(2)C_iC_{2v} + (2\gamma_v^c(2) - K_v^c(2)C_v)C_{2v} + \sum_{x=3}^{x_{max}}(\gamma_v^c(x) - K_v^c(x)C_v) - \sum_{x=3}^{x_{max}}(K_v^1(x)C_vC_{xi}) + Z_v\rho_d D_v(C_v^e - C_v) - \alpha C_vC_i - K_v^c(1)C_v^2 - K_v^1(2)C_vC_{2i}, \quad (14)$$

$$\frac{dC_{2v}}{dt} = \frac{1}{2}K_v^c(1)C_v^2 + \gamma_v^c(3)C_{3v} + K_v^c(3)C_iC_{3v} + \rho_d D_{2v}C_{2v}^e - K_v^cC_vC_{2v} - K_i^c(2)C_iC_{2v} - \gamma_v^c(2)C_{2v} - \rho_d D_{2v}C_{2v}, \quad (15)$$

$$\frac{dC_c(x)}{dt} = K_v^c(x-1)C_vC_c(x-1) - \{K_i^c(x)C_i + K_v^c(x)C_v + \gamma_v^c(x)\}C_c(x) + \{K_i^c(x+1)C_i + \gamma_v^c(x+1)\}C_c(x+1), \quad x = 3,4. \tag{16}$$

On the other hand, the equations representing single interstitials and interstitial clusters up to tetra-interstitials are given by

$$\frac{dC_i}{dt} = P_i + K_v^1(2)C_vC_{2i} - K_i^1(1)C_i^2 - \alpha C_vC_i - K_i^1(2)C_iC_{2i} - K_i^c(2)C_iC_{2v} - \sum_{x=3}^{x_{max}} K_i^1(x)C_iC_{xi} - \sum_{x=3}^{x_{max}} K_v^c(x)C_iC_{xv} - Z_i\rho_d D_iC_i, \tag{17}$$

$$\frac{dC_{2i}}{dt} = \frac{1}{2}K_i^1(2)C_i^2 + K_v^1(3)C_vC_{3i} - K_i^1(2)C_iC_{2i} - K_v^i(2)C_vC_{2i}, \tag{18}$$

$$\frac{dC_i(x)}{dt} = K_i^1(x-1)C_iC_1(x-1) + \gamma_v^1(x-1)C_1(x-1) - \{K_i^1(x)C_i + K_v^1(x)C_v + \gamma_v^1(x)\}C_1(x) + K_v^1(x+1)C_vC_1(x+1), \quad x = 3,4. \tag{19}$$

With the following definitions: $P_{v,i}$ = production rate of *surviving* Frenkel pairs (at/at/s), α = point defect recombination coefficient (s^{-1}) = $48\nu_i \exp(-E_M^i/kT)$, $K_{i,v}^{1,c}$ = rate constant for i/v impingement on loops/cavities (s^{-1}), ρ_d = dislocation density (m^{-2}), $D_{v,i}$ = point defect diffusion coefficients (m^{-2}), D_{2v} = di-vacancy diffusion coefficient (m^{-2}) = $\nu_v a^2 \exp\{-E_{2v}^m/kT\}$, and C_{2v}^e = di-vacancy thermal concentration (at/at/s) = $6\exp\{-(2E_F^v - E_B^{2v})/kT\}$. Di-vacancies are assumed to be mobile, and to interact mainly with dislocations. The definitions of the parameters in the equations and their numerical values for steel are given in Table I. The sets of balance Eqs. (14)–(19) are easily derived by considering production and destruction rate processes for a particular cluster size. Only 4 single rate equations for interstitial clusters and 4 similar equations for vacancies are used in this work. Larger size interstitial loops and cavities are characterized using Fokker–Planck continuum equations, as described below.

TABLE I Input parameters for 316 stainless steel

Symbol	*Parameter*	*Numerical value*
a^2/D_i	Recombination combinatorial number	48 [14]
$L_i^I(1)$	Interstitial–interstitial combinatorial number	84 [10]
$L_v^c(1)$	Vacancy–vacancy combinatorial number	84 [10]
E_v^m	Migration energy of a single vacancy	2.24×10^{-19} J [15]
E_i^m	Migration energy of a single interstitial	3.2×10^{-20} J [15]
E_v^f	Formation energy of a vacancy	2.56×10^{-19} J [15]
E_i^f	Formation energy of an interstitial	6.54×10^{-19} J [15]
E_{2v}^B	Migration energy of a di-vacancy cluster	1.44×10^{-19} J [15]
E_{2v}^B	Binding energy of a di-vacancy cluster	4×10^{-20} J [15]
E_{3v}^B	Binding energy of a tri-vacancy cluster	1.2×10^{-19} J [15]
a	Lattice parameter	3.63×10^{-10} m [10]
ν_i	Frequency factor for an interstitial	5.0×10^{12} [17]
ν_v	Frequency factor for a vacancy	5.0×10^{13} [17]
Z_v	Vacancy-dislocation bias factor	1.0 [15]
Z_i	Interstitial-dislocation bias factor	1.08 [15]
g	Surface energy	1 J/m^2 [15]

3.3 Fokker–Planck (F–P) Description of Large Loops

For the purpose of simplifying the analysis, we introduce the following notations:

$\kappa_l(x) = \gamma_v^I(x) + \beta_i^I(x)$ = Growth rate of an interstitial cluster by either vacancy emission ($\gamma_v^I(x)$) or interstitial impingement ($\beta_i^I(x)$),

$\kappa_v(x) = \beta_v^c(x)$ = Growth rate of a vacancy cluster by vacancy impingement,

$\lambda_v(x) = \beta_v^I(x)$ = Decay rate of an interstitial cluster by vacancy impingement,

$\lambda_c(x) = \gamma_v^c(x) + \beta_i^c(x)$ = Decay rate of a vacancy cluster by either vacancy emission or interstitial impingement,

where the impingement rates are given by

$$\beta_{v,i}^{c,I} = K_{v,i}^{c,I} C_{I,c}. \tag{20}$$

Equation (16) for a vacancy cluster and Eq. (19) for an interstitial cluster of any size "x" can now be lumped into one rate equation

$$\frac{dC_{I,c}(x)}{dt} = \kappa_{I,c}(x-1)C_{I,c}(x-1) - [\kappa_{I,c}(x) + \lambda_{I,c}(x)]C_{I,c}(x) + \lambda_{I,c}(x+1)C_{I,c}(x+1), \quad x > 4. \tag{21}$$

Dropping the cluster subscript (l,c) and expanding the first and last terms of Eq. (21) in a Taylor series up to the second term, Wolfer *et al.* [11] showed that the set of equations (19) can be replaced by one continuum equation of the form

$$\frac{\partial C}{\partial t} = -\frac{\partial}{\partial x}\left\{FC - \frac{\partial}{\partial x}(DC)\right\}, \tag{22}$$

where C is a generalized concentration for both types of point defect clusters and the "drift" function is defined as:

$$F(x,t) = \kappa(x,t) - \lambda(x,t) = \text{Net point defect bias flux.} \tag{23}$$

And the "diffusion" function by

$$D(x,t) = \tfrac{1}{2}\{\kappa(x,t) + \lambda(x,t)\} = \text{Average point defect bias flux.} \tag{24}$$

The last equation is used to represent both vacancy and interstitial clusters, with the appropriate F and D functions, for sizes containing more than four atoms. Equation (22) is the well-known form of the Fokker–Planck equation that describes diffusion in a drift field [18].

3.4 Solution Methods of the F–P Equation

The Fokker–Planck formulation presented by Eq. (22) has been the subject of investigation in various areas of physics [18–20], especially the physics of a non-equilibrium system of particles [18]. This equation describes the combined time-dependent nucleation and growth regimes of the microstructure. However, even with the simplest initial and boundary conditions, the equation proved to be difficult to solve analytically in its general form [19,20]. We will, in the following, introduce two methods for solving the F–P equation in the present one-dimensional case, and in later sections show how these methods can be extended to more general clustering problems.

Direct Numerical Methods

Since the F–P equation is a partial differential equation (PDE), many numerical methods can be used to solve it. We discuss here one direct

method of solution, based on transformation of variables and finite difference schemes. To realistically define the behavior of the microstructure at large irradiation doses, we introduce a new variable that is related to the defect radius by a logarithmic transformation

$$u = \ln(2r/b), \tag{25}$$

where r is the cluster radius and b is the Burgers vector. Also, let us define the following quantities: $n=2$ for loops, $n=3$ for voids; $B_2=\Omega/\pi b$ for loops, $B_3=3\Omega/4\pi$ for voids, where $\Omega\approx b^3=$ atomic volume, $x_l=$ number of interstitials in an interstitial loop, $x_c=$ number of vacancies in a cavity, $r_l=$ interstitial loop radius, and $r_c=$ cavity radius. The following relationships can then be easily verified

$$r_c = (3\Omega x_c/4\pi)^{1/3}(B_3 x_c)^{1/3} = \tfrac{1}{2} b e^{u_c}, \tag{26}$$

$$r_l = (\Omega x_l/\pi b)^{1/2} = (B_2 x_l)^{1/2} = \tfrac{1}{2} b e^{u_l}, \tag{27}$$

or generally, for both cavities and loops

$$r = (B_n x)^{1/n} = \frac{1}{2} b e^{u} \quad \text{and} \quad u = \frac{1}{n}\ln\left(\frac{2}{\pi} n x\right). \tag{28}$$

Using: $\dfrac{\partial}{\partial x} = \dfrac{\partial}{\partial u}\dfrac{\partial u}{\partial x} = \dfrac{1}{nx}\dfrac{\partial}{\partial u} = \dfrac{2}{\pi} e^{-nu}\dfrac{\partial}{\partial u}$, we obtain the following equation:

$$\frac{\partial C}{\partial t} = -\frac{2}{\pi} e^{-nu}\left[\frac{2}{\pi} e^{-nu}\left(\frac{\partial^2 (DC)}{\partial u^2} - n\frac{\partial (DC)}{\partial u}\right) - \frac{\partial (FC)}{\partial u}\right]. \tag{29}$$

Equation (29) is quite general and shows independence of the cluster type, except through D, F and n. A numerical solution of Eq. (29) is sought at discrete values of the variable u, where the partial derivatives are replaced by central finite differences. With the discrete values of u defined by $u(k)=(k-4)h+u(4)$, $k\geq 4$. And two new discrete functions defined by $\Psi(k,j)=(2e^{-nu(k)}/\pi h)^2 D(j)=$ Diffusion function; and $\Phi(k,j)=(2n/\pi^2 h)e^{-2nu(k)}D(j)+(1/\pi h)e^{-nu(k)}F(j)=$ Diffusion-drift function, and h the step size, we obtain the following set of discretized equations:

$$\begin{aligned}\frac{dC(k)}{dt} =& \{[\Psi+\Phi](k,k-1)\}C(k-1,t) - 2\Psi(k,k)C(k,t) \\ &+ \{[\Psi+\Phi](k,k+1)\}C(k+1,t).\end{aligned} \tag{30}$$

In comparing the results of numerical analysis with experimental data, however, one would be interested in characterizing parameters such as the total defect density, the average radius of both loops and cavities and the dislocation density for loops or sink strength for cavities. The total concentration of interstitial loops per unit volume $N_{\text{tot}}(t)$ is given by

$$N_{\text{tot}}(t) = \frac{1}{\Omega}\int_0^{\infty} C(x,t)\,\mathrm{d}x \approx \frac{1}{\Omega}\sum_{x=2}^{x_{\max}} C(x,t)\Delta x, \quad \Delta x \geq 1, \tag{31}$$

$$N_{\text{tot}}(t) \doteq \frac{2\pi}{\Omega b^2}\sum_{r_{\min}}^{r_{\max}} C(x,t) r\,\Delta r. \tag{32}$$

The average radius of an interstitial loop is given by

$$\bar{R}_1 \simeq \sum_{r_{\min}}^{r_{\max}} C(r,t) r^2\,\Delta r \Bigg/ \sum_{r_{\min}}^{r_{\max}} C(r,t) r\,\Delta r. \tag{33}$$

This numerical approach allows the study of defects containing up to millions of atoms with very modest computational requirements. Microstructure parameters, such as total defect concentration, average size, defect distribution and moments, and total sink strength can be calculated as functions of irradiation time. The results for the present hybrid approach have been compared to previous detailed rate theory computations. Various mesh sizes of the discretized Fokker–Planck equation resulted in size distributions that compare well with rate theory calculation [21]. Using material parameters representative of nickel (or stainless steel), shown in Table I, a numerical simulation of various dose rates is carried out. The concentrations of small size defect clusters is found to reach equilibrium values after ~ 100 s of irradiation. However, large size interstitial loops continue to develop with time, as can be seen from Fig. 1.

A correlation with experimental data on heavy ion irradiated 316 stainless steel at 10^{-3} dpa/s was finally conducted by Ghoniem and Sharafat [5]. The numerical values obtained from the present model were shown to match reasonably well with the experimental data of Williams on ion-irradiated steel at 673 and 873 K. Interstitial loop fractional concentrations are found to be smaller by 1–2 orders of magnitude at 873 K when compared to 773 K. The total loop concentration and

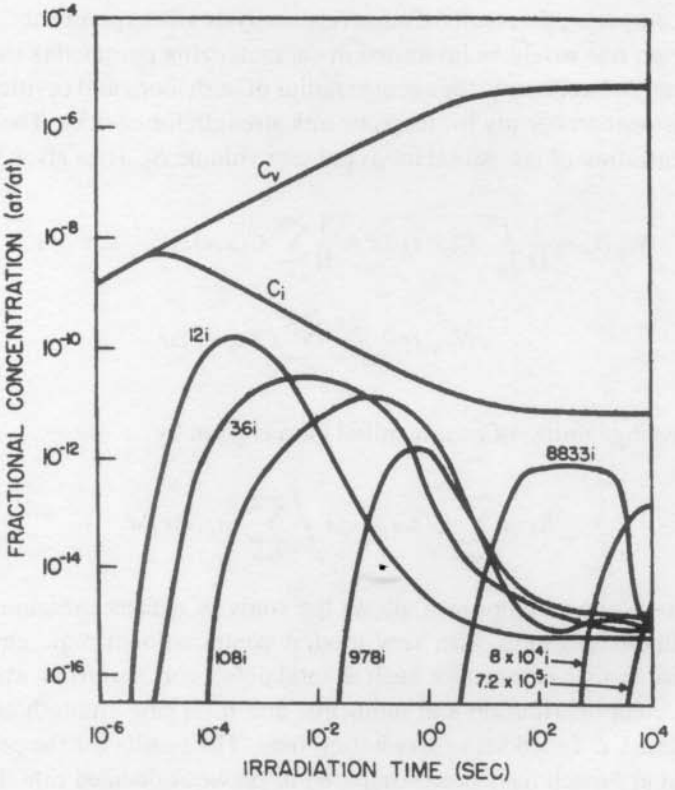

FIGURE 1 Time dependence of interstitial loop clusters at 873 K and 10^{-3} dpa/s.

dislocation loop line density are found to decrease, while the average size increases with increasing irradiation temperature, which is qualitatively consistent with fission reactor experiments.

Total interstitial loop concentrations, average radii and total dislocation line densities were shown to be in reasonable agreement with the experimental data. This can be inspected in Figs. 2 and 3. Moreover, the qualitative behavior of the microstructure, displayed in Figs. 1–4, shows the following trends:

(a) The concentration and density of dislocation loops decrease with increasing temperature at the same dose and dose rate.
(b) For a fixed irradiation temperature and dose, the loop concentration and dislocation density increase rapidly with dose rate.

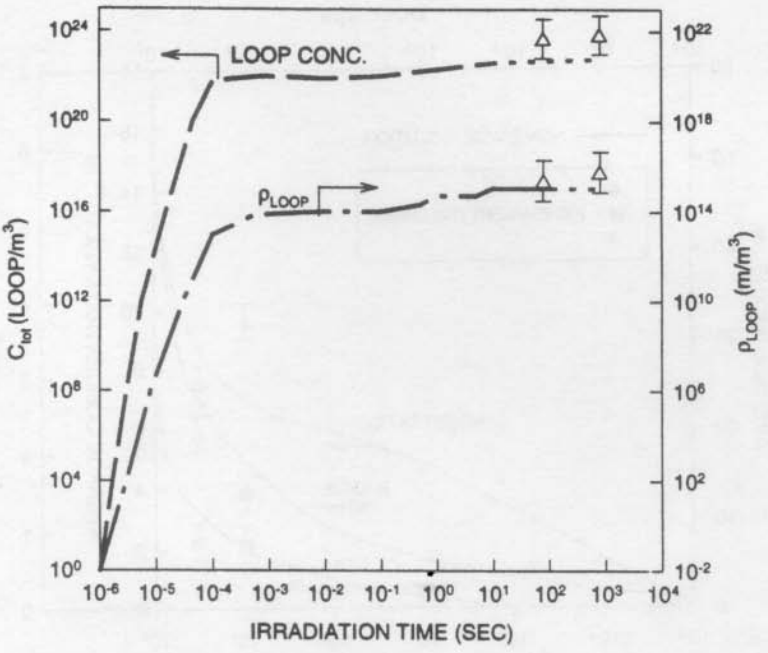

FIGURE 2 Comparison between theory and experiments (Williams) for loop concentration and dislocation density at 673 K and 10^{-3} dpa/s.

(c) The average loop size increases with increasing temperature at the same dose and dose rate, but decreases slightly with increasing dose rate if the total irradiation dose and temperature are constant.
(d) The growth speed of the interstitial loop distribution increases with increasing temperature.

The previous qualitative features are consistent with experimental data obtained from fission reactor [22] and simulation facilities [23], as shown in Fig. 2.

Direct numerical solutions to the F–P equation can be challenging because of the vast time and cluster space, which must be accurately covered. Different approaches to the solution of the F–P equation have been developed for a variety of applications. In this section, we outline one such method, which is based on the development of equivalent

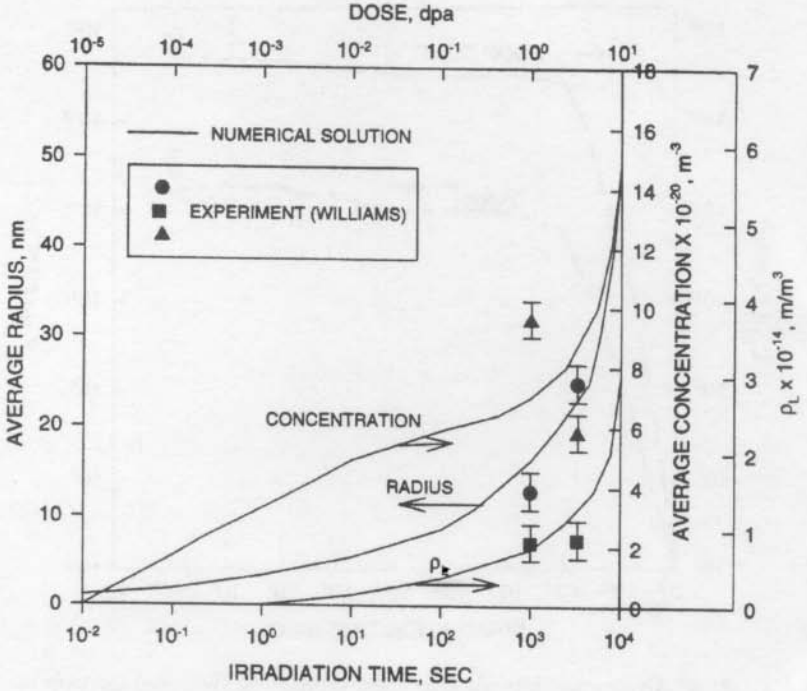

FIGURE 3 Comparison between theory and experiments of interstitial loop parameters at 873 K and 10^{-3} dpa/s.

kinetic equations for the moments of the distribution function. We also apply this technique to the evolution of interstitial loops in irradiated materials. The procedure has the advantage that it can be extended to more complex clustering problems, such as the formation of bubbles or complex phases in irradiated materials.

The moments method has been successfully used for the approximate determination of distribution functions, when described by partial or integro-differential equations, as in the work of Sigmund [23] and in that of Clement and Wood [24]. The zeroth moment of Eq. (22) gives

$$\frac{dN}{dt} = J^*, \tag{34}$$

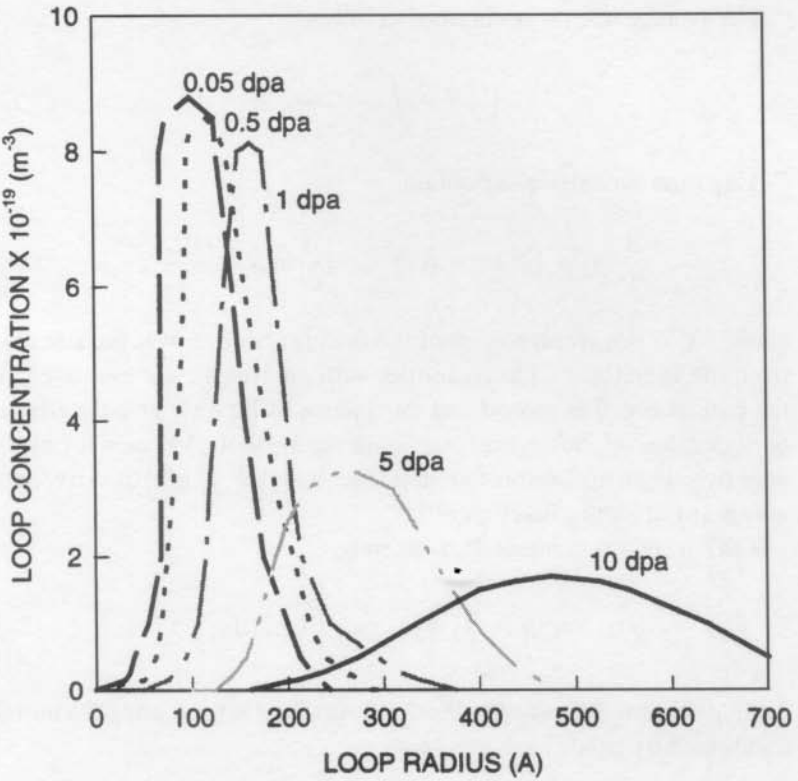

FIGURE 4 Evolution of the interstitial loop size distribution at high dose rates.

where

$$N = \int_{x^*}^{\infty} C \, dx \tag{35}$$

and is readily obtained by the direct integration of Eq. (34). N is the total density of atomic clusters, regardless of their size. The upper bound has been approximated as ∞ for mathematical simplicity. Solution to the second-order parabolic partial differential Eq. (22) is possible, provided the following boundary and initial conditions are satisfied:

$$\begin{aligned} C(\infty, t) &= 0, \\ C(x^*, t) &= C_{2i}(t) \equiv C^*, \end{aligned} \tag{36}$$

or, $J(x^*, t) = J^*$, and $C(x, 0) = 0$, $x > x^*$.

The average size $\langle x \rangle$ is obtained as follows:

$$\langle x \rangle N = \int_{x^*}^{\infty} xC \, \mathrm{d}x.$$

Taking time derivatives, we obtain

$$\frac{\mathrm{d}}{\mathrm{d}t}\langle x \rangle = \langle \Im(x) \rangle - (\langle x \rangle - x^*)\frac{\mathrm{d}}{\mathrm{d}t}\ln N + \frac{D^*C^*}{N}, \tag{37}$$

where $\langle \Im \rangle$ is the average value of the drift function $\Im$ over the size distribution function C. The quantities with an asterisk are evaluated at the critical size. The second and third terms of Eq. (37) give the effects of nucleation on the average size. Here the symbol $\langle\ \rangle$ is used for averages over the distribution function, i.e., $\langle \eta(x) \rangle = \int_0^x \eta(x) C(x) \, \mathrm{d}x$, and $\eta(x)$ is any arbitrary function of x.

The rth central moment M_r is given by:

$$M_r N = \int_{x^*}^{\infty} (x - \langle x \rangle)^r C(x, t) \, \mathrm{d}x. \tag{38}$$

Taking the time derivatives of both sides of Eq. (38) and using the initial and boundary conditions, we obtain:

$$\begin{aligned}\frac{\mathrm{d}M_r}{\mathrm{d}t} = {} & r\langle F(x - \langle x \rangle)^{r-1} \rangle + r(r-1)\langle D(x - \langle x \rangle) \rangle \\ & + r\frac{D^*C^*}{N}(x^* - \langle x \rangle)^{r-1} + \frac{\mathrm{d}}{\mathrm{d}t}(\ln N)[(x^* - \langle x \rangle)^r - M_r] \\ & - rM_{r-1}\frac{\mathrm{d}}{\mathrm{d}t}\langle x \rangle.\end{aligned} \tag{39}$$

Substituting for $\mathrm{d}\langle x \rangle / \mathrm{d}t$, a general equation for the rth moment can be derived:

$$\begin{aligned}\frac{\mathrm{d}M_r}{\mathrm{d}t} = {} & r[\langle F(x - \langle x \rangle)^{r-1} \rangle - M_{r-1}\langle F \rangle] + r\frac{D^*C^*}{N}\left[(x^* - \langle x \rangle)^{r-1} - M_{r-1}\right] \\ & + \frac{\mathrm{d}}{\mathrm{d}t}\left[(\ln N)(x^* - \langle x \rangle)^r - M_r - rM_{r-1}(x^* - \langle x \rangle)\right] \\ & + r(r-1)\langle D(x - \langle x \rangle)^{r-2} \rangle.\end{aligned} \tag{40}$$

Now let us define the nucleation functions ξ_r, the distortion functions Φ_r, and the dispersion functions ψ_r as,

$$\begin{aligned}
\xi_1 &= \frac{D^*C^*}{N} - (\langle x\rangle - x^*)\frac{\mathrm{d}}{\mathrm{d}t}\ln N,\\
\xi_r &= \frac{D^*C^*}{N} - \left[(x^* - \langle x\rangle)^{r-1} - M_{r-1}\right]\\
&\quad + \frac{\mathrm{d}}{\mathrm{d}t}(\ln N)\left[(x^* - \langle x\rangle)^r - M_{r-1}rM_{r-1}(x^* - \langle x\rangle)\right],\\
\Phi_r &= r\left[\langle F(x - \langle x\rangle)^{r-1}\rangle - M_{r-1}\langle F\rangle\right],\\
\psi_r &= r(r-1)\langle D(x - \langle x\rangle^{r-2})\rangle.
\end{aligned} \tag{41}$$

The complete system of moment equations can now be described as,

$$\begin{aligned}
\frac{\mathrm{d}}{\mathrm{d}t}\langle x\rangle &= \langle F\rangle + \xi_1,\\
\frac{\mathrm{d}M_r}{\mathrm{d}t} &= \psi_r + \Phi_r + \xi_r, \quad r = 2, 3, \ldots, \infty.
\end{aligned} \tag{42}$$

Since the distribution function is not known *a priori*, averaging of functions can only be made in an approximate way. For an arbitrary function x, the average value over the distribution function is given by

$$\begin{aligned}
\langle\eta(x)\rangle &= \frac{1}{N}\int_{x^*}^{\infty}\eta C\,\mathrm{d}x\\
&= \frac{1}{N}\int_{x^*}^{\infty}\left[\eta(\langle x\rangle) + \frac{(x - \langle x\rangle)}{1!}\eta'(\langle x\rangle) + \cdots\right]C\,\mathrm{d}x,\\
\langle\eta(x)\rangle &= \eta(\langle x\rangle) + \sum_{k=2}^{\infty}\frac{M_k}{k!}\frac{\mathrm{d}^k\eta(\langle x\rangle)}{\mathrm{d}x^k}.
\end{aligned} \tag{43}$$

The dispersion function ψ_r is given by averaging the product of the diffusion coefficient and the quantity $(x - \langle x\rangle)^{r-2}$ over the distribution function. Thus

$$\psi_r = r(r-1)\left[D(x - \langle x\rangle)^{r-2} + \sum_{k=2}^{\infty}\frac{M_k}{k!}\frac{\mathrm{d}^k}{\mathrm{d}x^k}\left[D(x - \langle x\rangle)^{r-2}\right]\Big|_{\langle x\rangle}\right]. \tag{44}$$

The distortion function Φ_r is given by

$$\Phi_r = r\Bigg[\Im(\langle x\rangle)(x-\langle x\rangle)x^{r-1} + \sum_{k=2}^{\infty}\frac{M_k}{k!}\frac{\mathrm{d}^k}{\mathrm{d}x^k}\left[F(x-\langle x\rangle)^{r-1}\right]\Big|_{\langle x\rangle} - M_{r-1}\langle F\rangle\Bigg]$$
$$= \Bigg[\delta(r-1)F(\langle x\rangle) + \sum_{k=2}^{\infty}\frac{M_k}{k!}\frac{\mathrm{d}^k}{\mathrm{d}x^k}\left[F(x-\langle x\rangle)^{r-1}\right]\Big|_{\langle x\rangle} - M_{r-1}\left(F(\langle x\rangle) + \sum_{k=2}^{\infty}\frac{M_k}{k!}\frac{\mathrm{d}^k}{\mathrm{d}x^k}(F)\Big|_{\langle x\rangle}\right)\Bigg]. \quad (45)$$

The set of kinetic moment equations (42) can now be solved, together with a set of discrete rate equations (e.g. Eq. (19)) for small cluster sizes up to x^*. the size distribution can be readily re-constructed from the moments [4]. An application of this method to the conditions of ion irradiation is discussed in the next section, where the evolution of interstitial loops can be directly compared to experiments.

Comparison of Moment Solution with Experiments

Hall and Potter [25] performed ion irradiation experiments on Ni, Ni–Si, and Ni–Al alloys. A series of experiments were conducted, where 3-MeV Ni^{58+} ions were used to bombard samples at 465°C. The peak displacement damage rate in their experiments was 3×10^{-4} dpa/s. A standard set of defect properties has been used in calculations of the density of interstitial loops (see Table I) and their size distribution by the moment method.

The bulk of interstitial loop nucleation is achieved within a short irradiation transient, on the order of 0.0001 dpa, as can be seen from Fig. 5. The agreement with the experimental results of Hall and Potter is achieved for an effective interstitial migration energy of 0.55 eV, which includes a trapping energy of 0.35 eV. On the other hand, the average loop diameter is shown to increase with irradiation dose, and to be in good agreement with experiments. The effect of the di-interstitial binding energy on the growth speed of loops is shown in Fig. 6. Good agreement with experiments is obtained for a binding energy value of

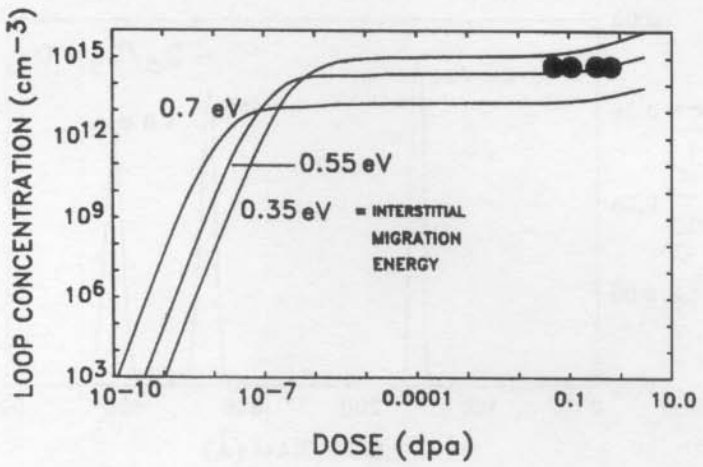

FIGURE 5 Dependence of interstitial loop concentration on irradiation dose for ion-irradiated nickel. Experimental data points are from Hall and Potter [25].

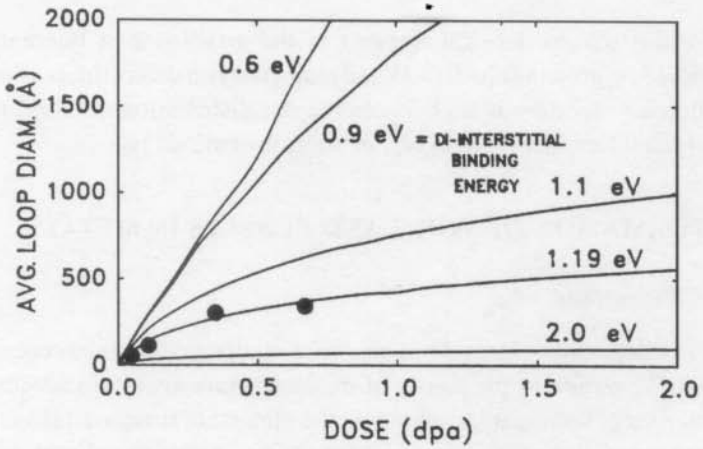

FIGURE 6 Comparison between theory (solid lines) and experiments (dots) [25] on the dose dependence of interstitial loop diameter in ion-irradiated nickel.

1.19 eV in this case. The distribution function of interstitial loops at 0.2, 1.0, and 1.8 dpa is shown in Fig. 7. In these calculations, only the effects of single step atomic transitions are considered. A comparison with experiments reveals that the spread of the size distribution is underestimated. Therefore, it is concluded that collision cascades play an

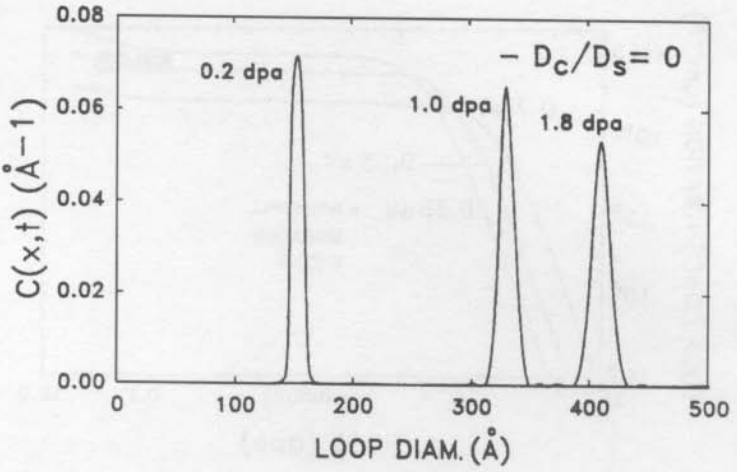

FIGURE 7 Distribution functions of interstitial loop size at various irradiation doses. Single step atomic fluctuations are assumed.

important role in the enhancement of the magnitude of fluctuations absorbed by growing clusters. When their effect on defect fluctuations is included, better agreement between the size distribution obtained from theory and that measured experimentally is obtained [4].

4 FORMATION OF VOIDS AND BUBBLES IN METALS

4.1 Background

The formation of voids and bubbles in irradiated materials has occupied a central position in the theory of microstructure evolution because of the impact of volumetric swelling on the lifetime of irradiated structural components. Traditionally, void formation in irradiated metals has been theoretically analyzed in two distinct phases: nucleation and growth. It has been implicitly assumed that the nucleation of voids is a fairly rapid process, followed by a slower growth phase. Void nucleation theories, as formulated by Katz and Wiedersich [26,27] and equivalently by Russell [28,29], have been motivated by the classical nucleation theory of droplet formation, developed earlier by Becker and Doring [30] and by Zeldovich [31]. Void growth, however, has been treated in the *mean field* approximation of identical spherical sinks that

grow in the diffusion fields of point defects. Many investigators have contributed to the rate theory of "average" void growth [32–37], and many features of experimentally observed cavity growth behavior were explained or predicted. However, this mean-field treatment of voids and bubbles is not adequate in general for a number of reasons, as given below:

(1) The continuous production of gas atoms and point defects is in contradiction with the termination of nucleation by a sudden decrease in the vacancy super-saturation, as assumed in classical nucleation theory.
(2) Classical nucleation theory predicts nucleation rates that are extremely sensitive to parametric variations, such as surface energy, super-saturation ratio and number of gas atoms within the cavity.
(3) Rate theory of cavity growth is unable to explain size and space distributions of cavities.

Application of the stochastic theory of defect clustering to the formation of voids and bubbles in irradiated materials has the advantage that there is no artificial separation between nucleation and growth. In addition, information on the size distribution of cavities would be readily available. Consider now the clustering of helium atoms and vacancies in gas-filled cavities. Each cluster will be containing varying numbers of helium atoms and vacancies. We will therefore be able to treat the problem in two-dimensional size space. Let us denote the cluster size by the vector $\boldsymbol{x}$, such that $\boldsymbol{x} = h\boldsymbol{e}_1 + v\boldsymbol{e}_2$. h and v are the number of helium atoms and vacancies in a cluster, respectively, and $\boldsymbol{e}_1$ and $\boldsymbol{e}_2$ are two unit vectors along the respective helium and vacancy directions. When the transition probability, W, and the cluster probability density, C, are both expanded around the point (h, v), one obtains the 2-D Fokker–Planck equation given by

$$\frac{\partial C}{\partial t} + \nabla \cdot J = 0, \tag{46}$$

where

$$J = FC - \nabla(DC), \tag{47}$$

$$F = \begin{bmatrix} a_{1h} \\ a_{1v} \end{bmatrix} \tag{48}$$

is a drift vector and,

$$D = \begin{bmatrix} a_{2hv} & a_{2hh} \\ a_{2vv} & a_{2vh} \end{bmatrix} \tag{49}$$

is a diffusion tensor. The first and second moments of the transition probability are given by the components of Eqs. (48) and (49). Details of the derivation of these equations can be found in [38]. It is noted, however, that while cascade-induced fluctuations do not affect the magnitude of the first moments (a_{1h} and a_{1v}), they increase the magnitudes of the second moments (a_{1hh} and a_{1vv}).

An approximate two-moment solution to the F–P equation is presented here for simplicity. Under these conditions, the rates of helium (k^{gc}), vacancy (k^{vc}) and interstitial (k^{ic}) capture, helium replacement (k^{gr}), and vacancy emission (k^{vc}) can be used to compute the elements of F and D. These are given by

$$a_{1h} = k^{\mathrm{gc}} - (k^{\mathrm{gc}} + k^{\mathrm{gr}}), \tag{50}$$

$$a_{1v} = k^{\mathrm{vc}}\left(k^{\mathrm{ie+ve}} + k^{\mathrm{gr}}\right), \tag{51}$$

$$a_{2hh} = \tfrac{1}{2}\left[k^{\mathrm{gc}} + k^{\mathrm{gr}} + k^{\mathrm{vc}}\right], \tag{52}$$

$$a_{2vv} = \tfrac{1}{2}\left[k^{\mathrm{ic}} + k^{\mathrm{gr}} + k^{\mathrm{vc}}\right], \tag{53}$$

$$a_{2hv} = a_{2vh} = k^{\mathrm{gr}}. \tag{54}$$

4.2 Approximate Two-moment Solution

The Fokker–Planck equation (Eq. (46)) must be solved for the evolution of the probability density, C, in order to determine the nature of the evolving HV clusters. A numerical solution, which is coupled with the transient nucleation conditions, has been developed by Sharafat and Ghoniem [38] for Eq. (46). Here, we present an alternate approximate two-moment solution method to the F–P equation, appropriate for the analysis of voids and bubbles in solids.

Taking the first moment of Eq. (46), we obtain

$$\frac{\mathrm{d}\langle x\rangle}{\mathrm{d}t} = \langle F(x)\rangle, \tag{55}$$

where the right-hand side represents the drift vector averaged over the probability distribution function. The symbol $\langle\ \rangle$ is used to denote this average. Equation (55) is not a closed equation because of the dependence of $\langle F \rangle$ on the unknown distribution function. However, to lowest order, one can approximate this equation by

$$\frac{\mathrm{d}\langle x \rangle}{\mathrm{d}t} = F(\langle x \rangle). \tag{56}$$

The integration of Eq. (56) gives the trajectory of the average cluster in the growth regime.

Let us define the variance matrix by

$$\langle \delta X_i \delta X_j \rangle = \langle X_i X_j \rangle - \langle X_i \rangle \langle X_j \rangle, \quad i,j = h, v. \tag{57}$$

It can be shown that kinetic equations for the variance matrix are given by

$$\frac{\mathrm{d}}{\mathrm{d}t} \langle \delta X_i \delta X_j \rangle = \langle X_i a_{ij} \rangle - \langle X_i \rangle \langle a_{ij} \rangle + \langle X_j a_{1i} \rangle - \langle X_j \rangle \langle a_{1i} \rangle + \langle a_{2,ij} \rangle. \tag{58}$$

Equation (58) is again not closed, and expansions of the parameters around their values at the average trajectory, $\langle x \rangle$, would result in an open-ended set of moment equations. Although it is possible to develop coupled equations for higher order moments (see [4]), it is sufficient here to develop a lowest order expansion of Eq. (58)

$$\frac{\mathrm{d}}{\mathrm{d}t} \langle \delta X_i \delta X_j \rangle \cong a_{2,ij}(\langle x \rangle). \tag{59}$$

Equation (59) is the lowest order evolution equation for the variance matrix. The second moments of the transition probabilities, $a_{2,ij}$, are the components of the diffusion tensor, and are to be evaluated at the average trajectory x.

We will proceed here by reconstructing the probability density function from its zeroth, first, and second moments. The simplest reconstruction procedure can be based on Gaussian functions, i.e.,

$$C(h, v, t) \cong \left(\delta X_h \delta X_v \sqrt{2\pi}\right)^{-1} \exp\left(-y^2/2\right), \tag{60}$$

where

$$y = \left[\left(\frac{h - \langle h \rangle}{\delta X_h} \right)^2 + \left(\frac{v - \langle v \rangle}{\delta X_v} \right)^2 \right]^{1/2} \tag{61}$$

4.3 Comparison with Experiments

Figure 8 shows a comparison between the results of theoretical calculations and the experimental size distribution of helium bubbles in irradiated 316 stainless steel under the conditions of the High Flux Irradiation Reactor (HFIR) at 14.3 dpa, and at 450°C. The experimental data are represented by the histogram, and are obtained from [39]. The agreement between theory and experiments is achieved by considering the influence of collision cascades on the fluctuations in atomic defect absorption. Figure 9 shows another comparison between theory and dual ion beam irradiation experiments for the total concentration of helium bubbles. The parameter B in the figure corresponds to the ratio of atomic displacements to helium re-solution back into the matrix.

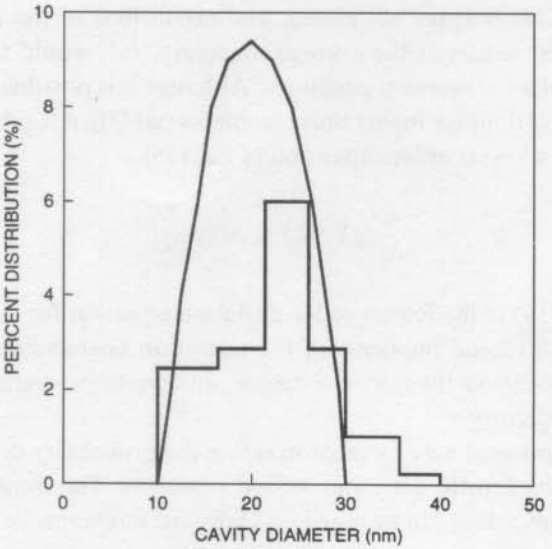

FIGURE 8 A Comparison between computed and experimentally measured cavity size distribution (histogram) at 14.3 dpa under HFIR irradiation conditions at 450°C.

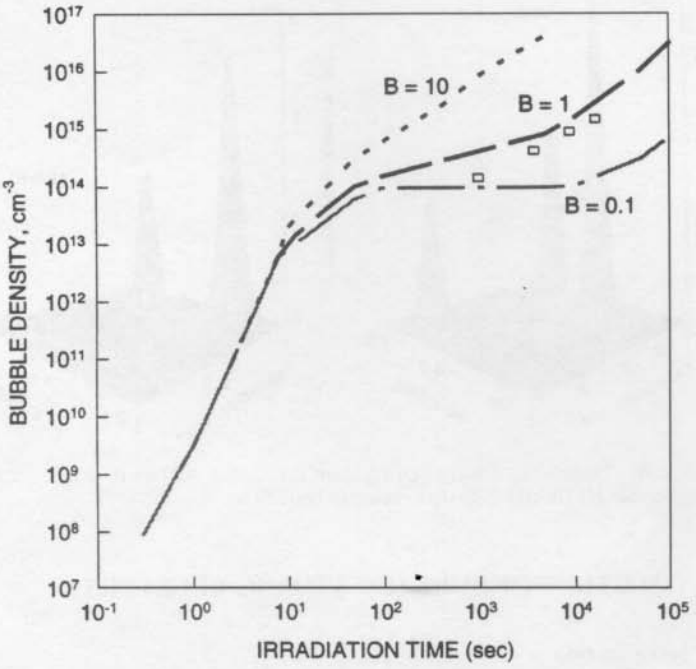

FIGURE 9 Comparison between theory and experiment on dual ion beam irradiation at a displacement rate of 3×10^{-3} dpa/s. The helium-to-dpa ratio is 5, and the data is taken from the work of Ayrault *et al.* [40].

Note that the best fit to the experimental data is obtained when $B = 1$ (i.e. helium in bubbles is displaced at nearly the same rate as matrix atoms.

The ratio of helium generation to the production of atomic defects during irradiation is a significant measure of the effects of helium on the microstructure. The He-to-dpa ratio is defined as the ratio of helium generation rate (appm/s) to displacement damage rate (dpa/s). For the HFIR, this ratio is 57, while it is of the order of 0.1 for the Experimental Breeder Reactor (EBR-II). In Fig. 10, the probability distribution functions for bubbles under HFIR and under EBR-II irradiation conditions in steel are shown. The low He-to-dpa ratio characteristic of EBR-II results in a much smaller spread in the size distribution in the helium direction, as compared to HFIR conditions. This indicates that gas-filled cavities in EBR-II are mostly voids, while they tend to be near equilibrium bubbles in the case of HFIR.

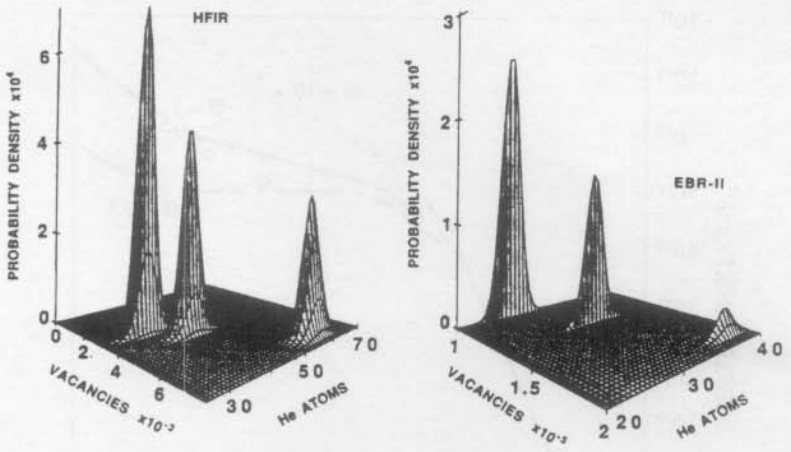

FIGURE 10 Probability distribution function for helium bubbles in irradiated stainless steel under HFIR and EBR-II irradiation conditions.

5 EVOLUTION OF SURFACE ATOMIC CLUSTERS

5.1 Introduction

The general phenomenon of particle aggregation and clustering is encountered in many seemingly unrelated research fields. For example, this concept has been used to describe the particle size distribution in aerosol physics [41] and star cluster size in astrophysics [42]. Other examples are found in materials science (e.g., in thin film formation [42–44], swelling of nuclear fuel materials [45], metal clusters in metal vapor [46], and in expanding nozzle flows [47]). The one feature these systems have in common is that they may be characterized by the size distribution of aggregates or clusters.

Microscopic processes (e.g., aggregation, coalescence, dissociation, and evaporation) govern the shape of the size distribution of clusters and its evolution in time. To learn about these processes and their relative importance from the size distribution in a given system, it is necessary to understand their influence on the aggregation kinetics. This can be achieved via a detailed model that incorporates all potentially relevant processes and allows the calculation of the size distribution. In this section, we develop the kinetic equations for the aggregation of surface atomic clusters, describing the early stages of thin film growth.

5.2 Rate Equations

We consider here a system of clusters that are characterized by the number of their constituents (typically atoms). Other degrees of freedom, such as the shape of clusters, are disregarded. The mobility of atomic clusters on the surface is much higher than in the bulk, because surface diffusion rate is many orders of magnitude larger than that in the volume. Allowance is made for coalescence reactions where two clusters combine to form a large one that contains the sum of atoms of the two coalescing clusters.

Let $C_i(t)$ be the concentration of clusters consisting of i atoms at a given time t. Depending on the system considered, the concentration might be given as either the number of clusters per unit *volume* or per unit *area*. Then the rate of coalescence per unit volume (or per unit area) of an i-cluster with a j-cluster is given by $K(i,j)C_iC_j$, where $K(i,j)$ is a rate constant that, in the general case depends on the sizes of both coalescing clusters. A general conservation equation for the cluster concentrations may be written as

$$\frac{\partial}{\partial t}C_i = \frac{1}{2}\sum_{j=1}^{i-1} K(j, i-j)C_jC_{i-j} - \sum_{j=1}^{\infty} K(i,j)C_iC_j + Q_i, \qquad (62)$$

where Q_i denotes an external source rate per unit volume (or per unit area) of clusters (mostly monomers). In some systems, clusters may not be entirely stable but rather dissociate spontaneously into fragments. In that case, a term of the form

$$-\frac{1}{2}\sum_{j=1}^{i-1} F(j, i-j)C_i - \sum_{j=1}^{\infty} F(i,j)C_{i+j} \qquad (63)$$

must to be added to the right hand side of Eq. (62). Here $F(i,j)$ denotes the rate at which a cluster of $(i+j)$ atoms dissociates into two clusters of i and j atoms. Finally there may be a possibility that clusters leave the system altogether (e.g., due to evaporation off a surface). This process may be accounted for by adding a term $(-v_iC_i)$ to the right-hand side of Eq. (62), where v_i is the loss rate of an i-size cluster. Equation (62), and its extensions by terms (63) and/or $(-v_iC_i)$ has been surveyed in some detail. Exact solutions are known for a few cases where the coalescence rate is a bilinear function of the cluster sizes.

To go beyond the limitations of these attempts, recourse to numerical techniques is necessary. Straightforward numerical time integration of Eq. (62) is possible, but the number of equations to be taken into account may become very large, especially at large times. Another method of solution is a direct Monte Carlo simulation [48,49].

5.3 Two-group Approach

We wish here to establish a method of solution for the agglomeration equation Eq. (62). The method is based on separating the clusters into two groups according to size: the first containing clusters with up to x^* atoms, and the second containing clusters with more than x^* atoms. The quantity x^* is some small integer that may be suggested, in some cases, by physical properties of the clusters (e.g., their stability). For the first group, a set of discrete equations describes the concentrations of individual cluster sizes; the second group is characterized by a set of equations for the moments of the distribution. In the work of Ghoniem and Sharafat [4,5], only single atom transitions were considered. Here, we relax this restriction in the general formulation. Consequently, we do not approximate the evolution equation for large clusters by a Fokker–Planck equation, but instead aim at deriving moment equations from the original Eq. (62).

Introduce power moments N_k of the cluster size distribution according to

$$N_k(t) = \sum_{i=l}^{\infty} i^k C_i(t). \tag{64}$$

The concentration of all clusters irrespective of their size is denoted by $N_0(t)$ and $N_1(t)$ is the concentration of atoms contained in these clusters. Multiplying Eq. (62) by i^k and summing over all i, one obtains

$$\frac{\partial}{\partial T} N_k = \frac{1}{2} \sum_{i=1}^{\infty} \sum_{j=1}^{\infty} C_i C_j K(i,j) \times \left[(i+j)^k - i^k - j^k \right] + \sum_{i=1}^{\infty} i^k Q_i. \tag{65}$$

The intuitive meaning of this equation is clear by observing that, in a coalescence event between clusters of sizes i and j, the moment N_k changes by

$$(i+j)^k - i^k - j^k. \tag{66}$$

In the following we classify clusters into two groups of sizes, $i \leq x^*$ and $i > x^*$. For the large clusters we wish to use a continuous description so we write $C(x)$, instead of C_i, for $x = i > x^*$. Sums over C_i are replaced by integrals over $C(x)\,dx$ in the obvious way. Equation (62) then becomes, approximately, for the small clusters,

$$\frac{\partial}{\partial t} C_i = \frac{1}{2} \sum_{j=1}^{i-1} K(j, i-j) C_j C_{i-j} - \sum_{j=1}^{x^*} K(i, j-j) C_i C_j - \int_{x^*}^{\infty} dx\, K(i, x) C_i C(x) + Q_i. \tag{67}$$

Next we introduce moments M_k of the large cluster continuum,

$$M_k = \int_{x^*}^{\infty} dx\, x^k C(x). \tag{68}$$

These are approximately related to the full moments, N_k in Eq. (64), by

$$M_k = N_k - \sum_{i=1}^{x^*} i^k C_i. \tag{69}$$

Substituting Eq. (69) into the moment Eq. (65) and performing the separation, we obtain

$$\begin{aligned} \frac{\partial}{\partial t} M_k = &- \sum_{i=1}^{x^*} i^k \frac{\partial}{\partial t} C_i + \frac{1}{2} \sum_{i=1}^{x^*} \sum_{j=1}^{x^*} C_i C_j \times K(i, j) \left[(i+j)^k - i^k - j^k \right] \\ &+ \sum_{i=1}^{x^*} C_i \int_{x^*}^{x} dx\, C(x) K(i, x) \times \left[(i+j)^k - i^k - j^k \right] \\ &+ \frac{1}{2} \int_{x^*}^{\infty} \int_{x^*}^{\infty} dx\, dy\, C(x) C(y) \times K(i, x) \left[(x+y)^k - x^k - y^k \right] \\ &+ \sum_{i=1}^{\infty} i^k Q_i. \end{aligned} \tag{70}$$

Our final goal is to obtain from Eqs. (67)and (70) a closed set of equations for the small cluster concentrations C_i, $i = 1, 2, \ldots, x^*$, and the first

few continuum moments M_k, $k=0,1,\ldots,n$, where n is some small integer. To achieve this, we need to express the integrals over the continuum distribution in terms of the moments M_k.

Consider the quantity

$$G=\int_{x^*}^{\infty} \mathrm{d}x\, C(x)g(x), \tag{71}$$

where $g(x)$ is some arbitrary function. Our task is to obtain an approximate expression for G in terms of the moments M_k of Eq. (70). This problem is, of course, of a general nature, but its solution is not unique. An ingenious method to obtain bounds for G based on a representation of $C(x)$ by an array of delta functions is given in [50]. Here, however, we wish to use a somewhat simpler scheme which gives accurate results if the distribution $C(x)$ is fairly localized and if $g(x)$ varies only slowly.

Expand the function $g(x)$ in a Taylor series around some point x_0,

$$g(x)=\sum_{n=0}^{\infty}\frac{1}{n!}(x-x_0)^n g^{(n)}(x_0)=\sum_{n=0}^{\infty}\frac{1}{n!}g^{(n)}(x_0)\sum_{v=0}^{\infty}\binom{n}{v}x^v(-x_0)^{n-v}. \tag{72}$$

Inserting this expression into Eq. (71) gives the desired result,

$$G=\sum_{n=0}^{\infty}\frac{1}{n!}g^{(n)}(x_0)\sum_{v=0}^{n}\binom{n}{v}(-x_0)^{n-v}M_v. \tag{73}$$

Although Eq. (73) is valid for any expansion point, the preferable choice for x_0 is the average cluster size,

$$x_0-x^*=\bar{x}=M_1/M_0, \tag{74}$$

particularly so if the distribution $C(x)$ is uni-modal,

$$\frac{\partial}{\partial t}C_i=\frac{1}{2}\sum_{j=1}^{i-1}K(j,i-j)C_jC_{i-j}-\sum_{j=1}^{i-1}K(i,j)C_iC_j$$
$$-\sum_{n=0}^{\infty}\frac{1}{n!}K^{(0,n)}(i,\bar{x})C_i\times\sum_{v=0}^{n}\binom{n}{v}(-\bar{x})^{n-v}M_v+Q_i, \tag{75}$$

where the symbol $K^{(m,n)}$ denotes that partial derivative,

$$K^{(m,n)}(x,y) = \frac{\partial^{m+n}}{\partial x^m \partial y^n} K(x,y). \tag{76}$$

Equation (70) may be treated similarly, and the result of this procedure gives the following equation for the kinetic moments (see Ref. [53] for details):

$$\begin{aligned}\frac{\partial}{\partial t} M_k = &- \sum_{i=1}^{x^*} i^k \frac{\partial}{\partial t} C_i + \frac{1}{2} \sum_{i=1}^{x^*} \sum_{j=1}^{x^*} C_i C_j K(i,j)[(i+j)^k - i^k - j^k] \\ &+ \sum_{i=1}^{x^*} C_i \sum_{l=1}^{k-1} \binom{k}{l} i^{k-l} \sum_{n=0}^{\infty} \frac{1}{n!} K^{(0,n)}(i,\bar{x}) \sum_{v=0}^{n} \binom{n}{v} (-\bar{x})^{n-v} M_{l+v} \\ &+ \frac{1}{2} \sum_{l=1}^{k-1} \binom{k}{l} \sum_{m=0}^{\infty} \sum_{n=0}^{\infty} \frac{1}{m!n!} K^{(m,n)}(\bar{x},\bar{x}) \\ &\times \sum_{\mu=0}^{m} \sum_{v=0}^{n} \binom{m}{\mu} \binom{n}{v} (-\bar{x})^{m+n-\mu-v} M_{l+v} M_{k-l+\mu} \\ &+ \sum_{i=1}^{\infty} i^k Q_i. \end{aligned} \tag{77}$$

Equations (75) and (77) are coupled sets of non-linear ordinary differential equations for the small-size cluster concentrations and the continuum moments. If we take only the first two terms in the Taylor Series for $K(x,y)$ into account (i.e., we truncate all terms with $m,n \geq 2$), then the system is self-contained for any number of moments M_k, $k = 0, 1, \ldots, N$, with $N \geq 1$. Since the coalescence rate $K(x,y)$ is supposed to be a smooth function of size for large clusters, this truncation is not considered to be severe. We thus have a versatile tool to study numerically the kinetics of aggregation phenomena for a wide variety of physical systems.

5.4 Reconstruction of the Continuum Size Distribution

The general problem of reconstruction of distribution function from moments is well established and arises in various areas of research such as ion implantation [51]. A number of reconstruction schemes are

available which technically might be classified as linear and non-linear. In linear reconstruction, the function is expanded in a set of orthogonal functions where the expansion coefficients are determined by the moment constraints. Making use of the orthogonality relations, the result is obtained in closed form. One such well-known technique is the Gram–Charlier series expansion [52]. For functions close to Gaussian, this method gives quite satisfactory results for highly skewed functions, as will be shown here. One severe drawback inherent to all linear schemes is that the reconstructed curve may assume negative values, which is physically impossible for the true distribution function. Non-linear reconstruction schemes assume a certain form for the unknown function with adjustable free parameters to give the correct moments. This method is especially powerful if, for instance, theoretical considerations suggest some specific functional form. Certainly the reconstructed function can be *constrained* to be non-negative.

The most general non-linear reconstruction method may be obtained from the maximum entropy principle. The foundation of this principle has been given by Jaynes [53]. It provides the means to select an unbiased estimate in the sense of Bayes of the distribution given only the incomplete information of a finite set of expectation values (moments). In brief, the idea is to assign a function $C(x)$ that maximizes the entropy S, where S is defined as

$$S = -\int_{x^*}^{\infty} \mathrm{d}x\, C(x) \ln \frac{C(x)}{p(x)}, \tag{78}$$

and $C(x)$ satisfies the moment constraints. In Eq. (78), $p(x)$ denotes a prior probability or measure [52]. Roughly speaking, $p(x)\,\mathrm{d}x$ is proportional to the number of states within the interval $(x, x+\mathrm{d}x)$. In our case, the continuous variable x represents the number of atoms in a cluster, originally an integer, and thus we set $p(x)=1$. The entropy in Eq. (78) is maximized subject to the moment constraints given in Eq. (68), for $k=0, 1, \ldots, N$, by introducing Lagrange multipliers λk in the usual way, giving the result

$$C(x) = p(x) \exp\left(-\sum_{k=0}^{N} \lambda_k x^k \right). \tag{79}$$

Indeed, if no constraints were given at all, $N=0$, Eq. (79) would result in $C(x)=p(x)$ which is consistent, since $p(x)$ is the prior probability.

Equation (79) is a formal solution in the sense that the Lagrange multipliers λk have yet to be determined from the moment constraints,

$$\int_{x^*}^{\infty} \mathrm{d}x\, x^k \exp\left(-\sum_{l=0}^{N} \lambda_l x^l\right) = M_k, \quad k = 0, 1, \ldots, N. \tag{80}$$

Equation (80) comprises a non-linear system of equations for the λk that was solved numerically [53].

To validate the method, we use an example of the condensation of atoms deposited on a substrate surface as it occurs in the early states of thin film formation. For this system, an analytical solution is available [53]. In Fig. 11, we plot the distribution function together with the reconstruction from its moments by the maximum entropy principle. Good convergence is found even though the original distribution has a sharp peak and is highly skewed. The reconstructed curves oscillate somewhat around the true distribution, but the oscillation decays rapidly with increasing number of moments. The constrained maximum entropy principle gives a satisfactory reconstruction even of the sharp-peaked

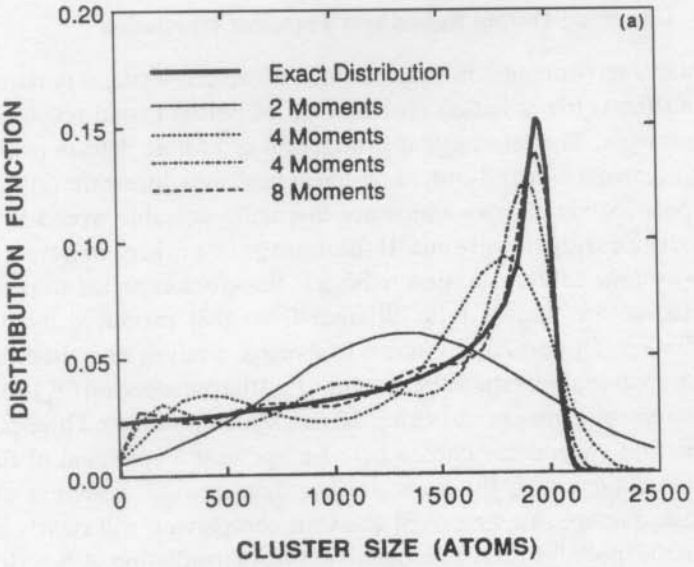

FIGURE 11 Reconstruction of the size distribution for constant monomer aggregation coefficient using exact moments (thick solid lines), and reconstruction (thin lines).

test function presented here. The method has been successfully used in the prediction of the early stages of thin film growth, including coalescence and ion bombardment processes [54,55].

6 SPACE–TIME INHOMOGENEITIES

The theoretical description presented in the previous section is adequate as long as the system is homogeneous both in time and space. Any situation, which may lead to breaking this space–time symmetry, is capable of carrying the system into totally different regimes of behavior. Many experimental observations on microstructure evolution have shown that drastic changes take place under pulsed or transient irradiation. Also, it has been experimentally observed that the microstructure tends to be highly organized in regular spatial patterns, even when the irradiation is steady. In this section, we explore first the effects of pulsed irradiation on microstructure evolution under spatially uniform conditions. This is followed by a presentation of spatial symmetry breaking results, and the formation of self-organized microstructure.

6.1 Clustering During Pulsed and Transient Irradiation

A unique environment in which atomic defect clustering is particularly interesting is the radiation environment of pulsed fusion reactors and accelerators. The intermittent production of atomic defects results in enhancement of second-order non-linear reactions during the on-time of the pulse, while clusters which are thermally unstable would tend to dissociate during the off-time. If the damage rate is kept to have a fixed time-average value, radiation pulsing is therefore expected to produce microstructure that is quite different from that produced by steady irradiation. Of particular interest to damage analysis of pulsed fusion reactor materials are the pulse on time (T_{on}) the pulse period (T_p) and the displacement damage rate during the irradiation pulse (P). Three pulsed irradiation systems are chosen here to represent a spectrum of fusion reactor designs with the same *average* damage rate. Selection of the average damage rate as a fixed basis for comparison will clearly bring about the special effects of the pulsed nature of irradiation. A description of the main parameters of the three pulsed systems is shown in Table II below.

TABLE II Parameters of selected pulsed radiation systems

Irradiation concept	T_{on} (s)	T_p (s)	P (dpa/s)
Magnetic confinement fusion reactor	224	245	10^{-6}
Simulation facility (pulsed ion accelerator)	10^{-3}	1	10^{-3}
Inertial confinement fusion reactor (ICFR)	10^{-6}	1	1

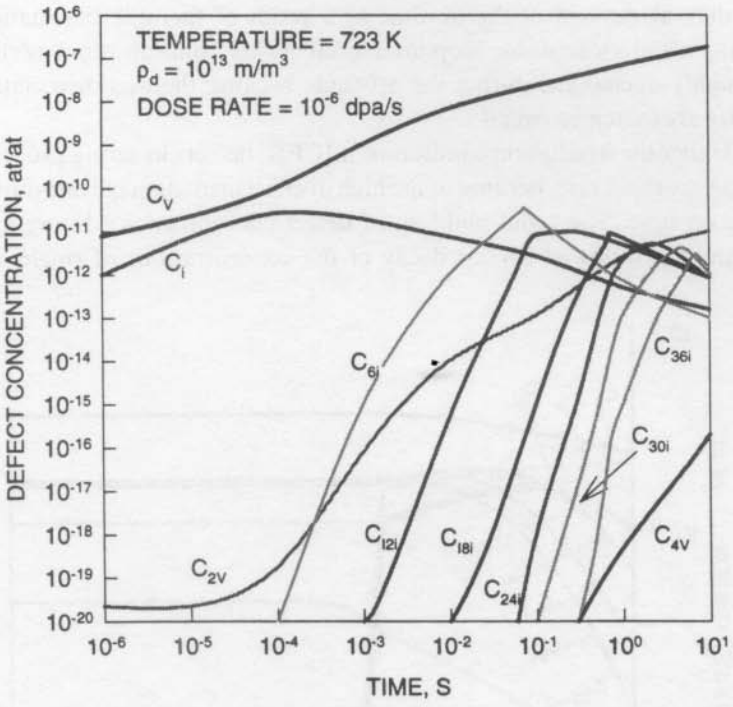

FIGURE 12 Time dependence of small micro-void and interstitial loop clusters for fusion reactor conditions.

The material parameters given in Table I are used in the following calculations. An irradiation temperature of 450°C and an initial dislocation density of 10^{13} m/m^3 are selected as reference conditions for the comparison. The time evolution of interstitial loops and micro-voids for typical Tokamak reactor irradiation conditions are shown in Fig. 12. For very short times (less than 10^{-4} s), the concentrations of single vacancies and interstitials increase linearly with time. As soon as diffusion sets in, point defects are absorbed at microstructure sinks, or they recombine with each other, thus modifying this linear dependence.

It is noted here that only a small fraction of single interstitial atoms end up in clusters, as interstitial loops. The nucleation and growth of self-interstitial clusters during the first on-time of a pulsed accelerator is shown in Fig. 13. The concentration of single interstitials peaks at 10 μs then decreases afterwards as a result of mutual recombination with vacancies. The concentration of di-interstitial clusters decreases immediately at the end of the on-time as a result of thermal dissociation. Larger and more stable loop interstitial cluster concentrations remain roughly unchanged during the off-time, because thermal dissociation rates are extremely small.

Under the irradiation conditions of ICFR, defect clustering proceeds at a very rapid rate, because of the high displacement damage rate during the on-time. The rapid build-up of defect concentrations during irradiation is followed by fast decay of the concentrations of single and

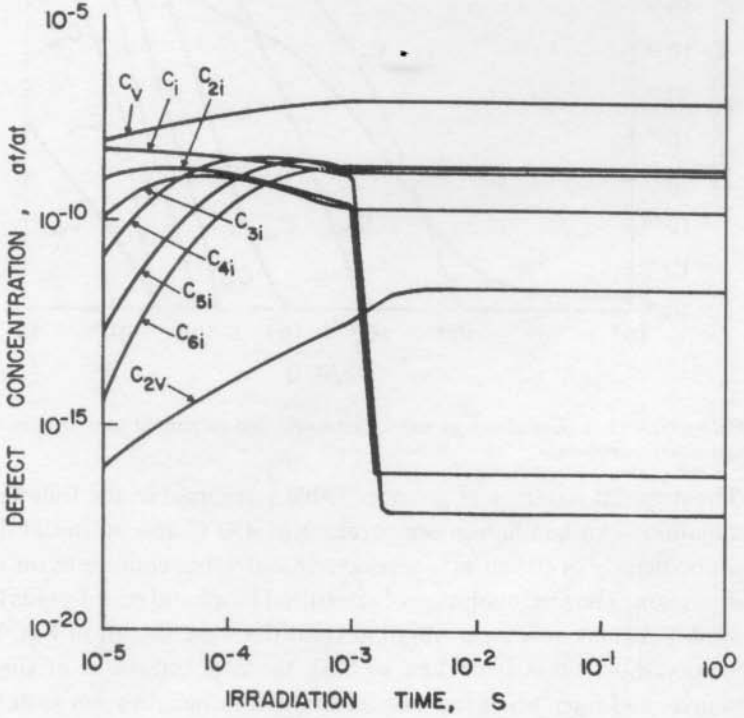

FIGURE 13 Defect cluster concentrations under the conditions of pulsed accelerators ($P = 10^{-3}$ dpa/s during 1 ms, and $T_p = 1$ s).

di-interstitials during the off period. Due to the extremely high displacement damage rate, as compared to the previous two irradiation cases, the concentration of small defect clusters is vastly enhanced. The average size of these clusters, however, is much smaller, because the total amount of displacement damage is kept the same on average.

Since the irradiation conditions of the Tokamak system are representative of steady irradiation, we will use it as reference. The effects of irradiation pulsing on change from this reference case will be explored here. The interstitial cluster size distributions for the three cases at the end of an accumulated dose of 7×10^{-6} dpa are shown in Fig. 14. It is noted that the size distribution in the highly pulsed case (ICFR) is more asymmetric than the other cases. At this dose, the peak size is only around 4 atoms in the ICFR case, 21 atoms for the pulsed accelerator and 34 atoms for the Tokamak. A comparison of the average loop size for the three systems is shown in Fig. 15. While the average loop size for the Tokamak increases almost linearly after the initial transient, the size develops almost in a "step function" fashion for the accelerator and ICFR cases. The total loop concentrations are shown as functions of irradiation time in Fig. 16. The loop concentration is shown to increase at a much higher rate in the two pulsed systems, as compared to the

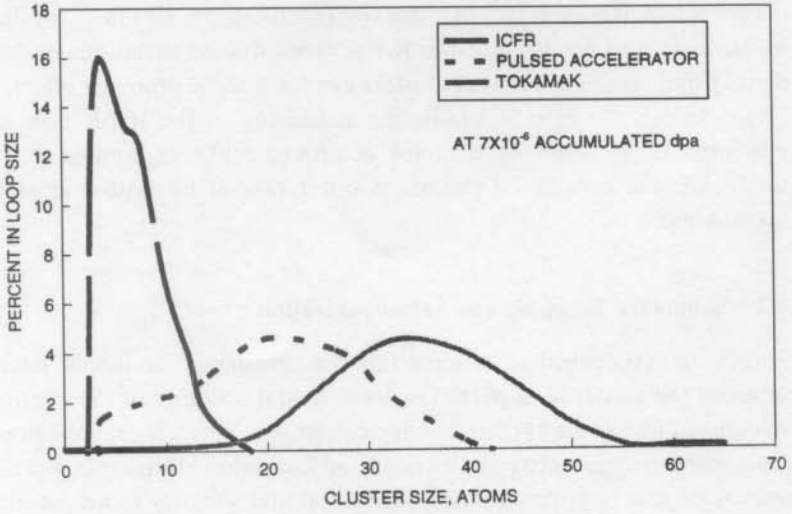

FIGURE 14 Intersitial cluster size distributions for Tokamak, pulsed accelerator and ICFR conditions at the end of an accumulated dose of 7×10^{-6} dpa.

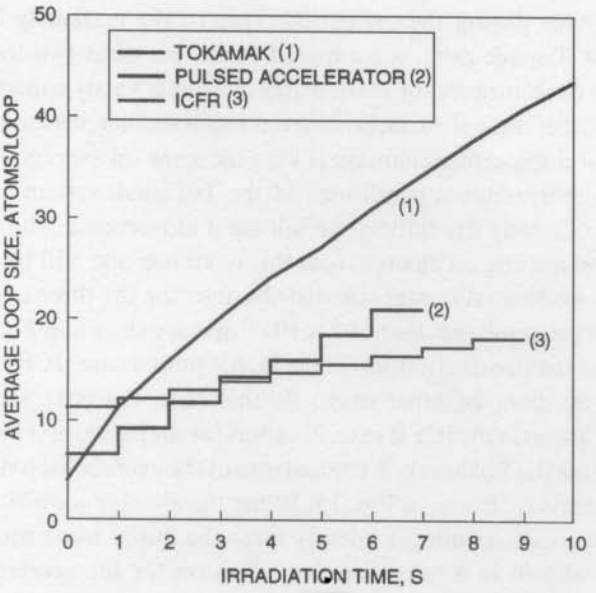

FIGURE 15 A comparison of the average interstitial loop size distributions for the three systems.

Tokamak case. After a short irradiation period of 10 s, the interstitial cluster concentration is $10^{16}\,m^{-3}$ for the Tokamak, $2 \times 10^{21}\,m^{-3}$ for the accelerator, and 4×10^{22} for the ICFR. Such drastic variations in the density and size of interstitial clusters can have some dramatic effects. For example, the rate of irradiation hardening in the ICFR case is predicted to be faster by a factor of almost 6000, as compared to the Tokamak, because of the much faster rate of interstitial cluster accumulation [56].

6.2 Symmetry Breaking and Self-organization

Numerous experimental observations on irradiated materials have revealed the existence of partial or total spatial ordering of the microstructure under a variety of irradiation conditions. This self-organization phenomenon appears to be influencing the formation of various types of microstructure (e.g. precipitates, interstitial and vacancy loops, voids, and bubbles). Complete isomorphism between the periodic structure and the underlying crystal lattice has been observed. However, the

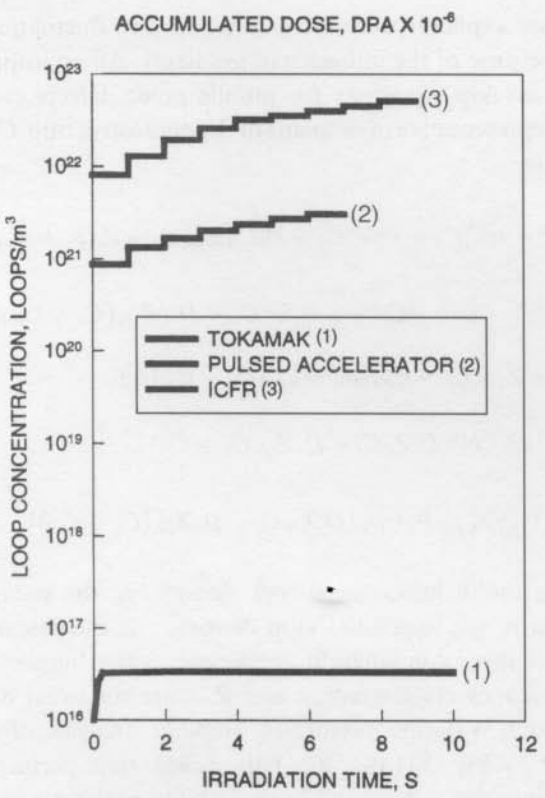

FIGURE 16 Time dependence of the total interstitial loop concentration in the three pulsed cases.

wavelength of the emerging microstructure pattern is typically 3 orders of magnitude larger than the lattice constant. Over the past several decades, experimental observations have been made on bubble [57,58] and void [59,60] lattices. More recently, systematic observations of defect ordering in ion-irradiated nickel and copper have shown the development of periodic defect walls. Strong anisotropic arrangements of stacking fault tetrahedra and vacancy-type clusters were observed by Jaeger and coworkers [61] in Cu on the {100} planes.

To account for the emergence of spatial patterns, we present here a model for the interaction between the microstructure and point defect diffusion fields. The model is based on the rate theory presented in the previous sections, and includes spatial diffusion operators. Thus, spatial

gradients are explicitly accounted for, and any fluctuations may be amplified because of the influence of gradients. An appropriate model here is to develop equations for mobile point defects coupled with equations representative of elements of the microstructure. Consider the model below.

$$\frac{\partial C_i}{\partial t} = P - \alpha C_i C_v + D_i \nabla^2 C_i - D_i C_i (Z_{iN}\rho_N + Z_{iv}\rho_v + Z_{il}\rho_I),$$

$$\frac{\partial C_v}{\partial t} = P(1-\varepsilon) - \alpha C_i C_v + D_v \nabla^2 C_v - D_v (Z_{vN}(C_v - C_{vN})\rho_N + Z_{vV}(C_v - C_{vV})\rho_V + Z_{vl}(C_v - \bar{C}_{vl})\rho_I), \tag{81}$$

$$\frac{\partial \rho_I}{\partial t} = (2\pi N/|b|)(D_i Z_{il} C_i - D_v Z_{vl}(C_v - \bar{C}_{vl})),$$

$$\frac{\partial \rho_V}{\partial t} = (1/|b| r_V^0)[\varepsilon P - \rho_V (D_i Z_{iV} C_i - D_v Z_{vV}(C_v - \bar{C}_{vl})),$$

where ρ_N is the dislocation network density, ρ_V the vacancy cluster density, and ρ_I the interstitial loop density. ε is the cascade collapse efficiency, α the recombination coefficient, b the burgers vector, r_0^V the mean vacancy cluster radius, and $Z\ldots$ are the usual bias factors. Ghoniem and Walgraef performed stability analysis of the model represented by Eq. (81) (see [62–64]). Space–time perturbations are introduced into this system, and linear stability analysis is performed. It is found that because of spatial fluctuations in point defect concentrations, the vacancy and interstitial loop cluster populations are unstable. A critical wavelength for self-organization is obtained in the form

$$\lambda_c = 2\pi \left[\frac{D_v(\bar{C}_{vV} - \bar{C}_{vN})}{(1+B)\varepsilon P \rho_N} \right]^{1/4}, \tag{82}$$

where $(1+B)$ is the dislocation bias factor, $\bar{C}_{vV}$ is the thermodynamic vacancy concentration near vacancy clusters, and $\bar{C}_{vN}$ is the thermodynamic vacancy concentration near dislocations. The wavelength predicted by Eq. (82) decreases with increasing the dislocation network density, cascade collapse efficiency, and displacement damage rate. These predictions are in accord with experimental observations [57–61].

In the weakly non-linear regime, fluctuations in point defect concentrations given by Eq. (81) can be expanded in a power series in vacancy

cluster density. This procedure is shown to lead to a Ginzburg–Landau type equation for the order parameter σ, representing space–time microstructure density profiles, of the form

$$\dot{\sigma} = \left[\left(\frac{b - b_c}{b_c}\right) - \xi_0^2(q_c^2 + \nabla^2)^2\right]\sigma + v\sigma^2 - u\sigma^3, \tag{83}$$

where $b = B/\varepsilon$, $\xi_0^2 = \rho_N/\rho_0$, $v = 2/(x_0)^{3/2}$, $u = 2/(x_0)^{5/2}$, and $x_0 = \rho_0/\rho_N$. The homogeneous solution for the loop density is ρ_0, b_c is the critical value of the bifurcation parameter at the instability, and $\bar{q}_c$ is the critical wave vector. Details of the theory can be found in [62–64].

Solution of Eq. (83) gives rise to spatial self-organization of the microstructure density order parameter σ. Figure 17 shows a direct

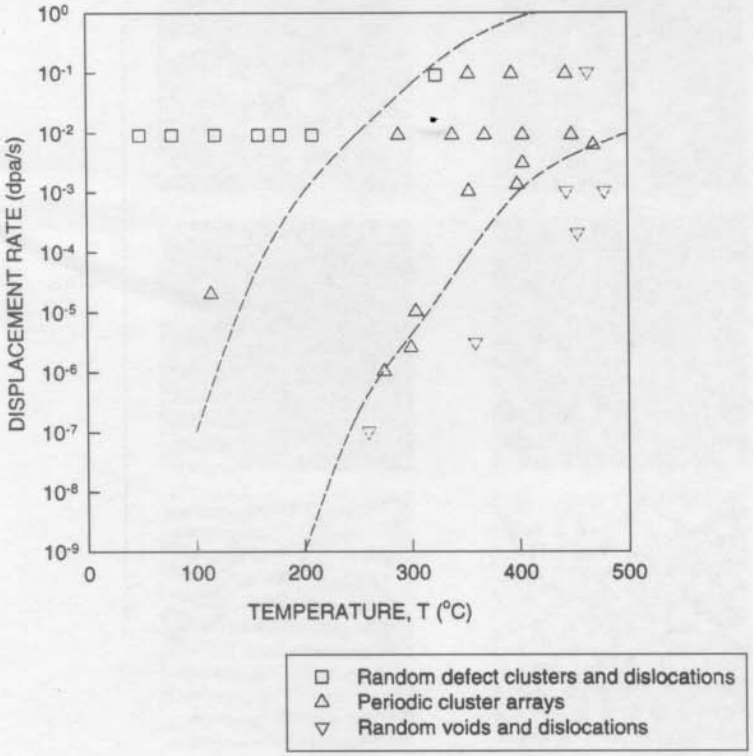

FIGURE 17 Comparison between theory and experimental data of ion-irradiated nickel [61]. The solid line represents the boundary between stable (random) void and dislocation arrays, and self-organized microstructure.

comparison between the theory and experimental data of ion-irradiated nickel [61]. The solid line is based on Eq. (82) for the onset of spatial instabilities, and represents the boundary between stable (random) void and dislocation arrays, and self-organized microstructure. The recombination limit (dashed line) is calculated by Abromeit and Wollenberger [65]. Figure 18 shows the steady-state solution to Eq. (83) for the spatial distribution of vacancy cluster densities. Agreement with the experimental work of Jaeger and coworkers [61] is readily achieved when a small degree of anisotropy in point defect migration is included.

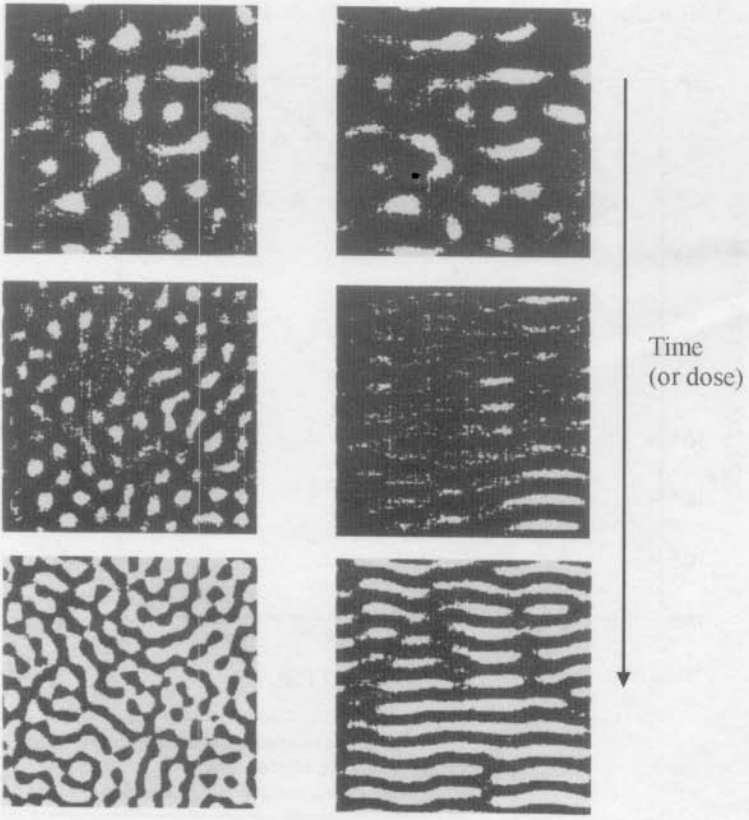

FIGURE 18 Computed time evolution of vacancy cluster patterns under irradiation. On the left column, isotropic point defect diffusion is assumed, while 1% anisotropy in interstitial diffusion is assumed on the right.

7 SUMMARY AND CONCLUSIONS

The theory of defect clustering under non-equilibrium conditions is deeply rooted in statistical physics, and is shown to bear fruitful results for the study of a variety of interesting physical phenomena. Starting from basic understanding of stochastic fluctuations in defect fields, it is shown that one can formulate master equations at the microscopic or atomic level. These equations can be treated in a more macroscopic sense by equivalent rate equations, in the limit of Poisson probability distributions for transitions between states. Under irradiation, diffusion in the bulk of large defect clusters is slow, and the transitions between states are shown to be just between nearest neighbors. A useful approximation is obtained, which is shown to be the Fokker–Planck continuum theory. Several solution methods have been presented for a hybrid scheme that links the rate equations with the continuum F–P equation. The method of moments is particularly useful, because it is relatively simpler than other numerical methods. In addition, the method allows for direct comparison with experiments on the evolution of the size distribution of defect clusters. The theory is shown to be successful in explaining experimental observations on size distributions of interstitial loops under irradiation. The influence of collision cascades is shown to be important, and results in increased dispersion of the size distribution probability function.

The evolution of vacancy and interstitial clusters is shown to proceed on two different time scales. While interstitial clusters form very rapidly, the time scale for the formation of vacancy clusters is many orders of magnitude longer, mainly reflecting the magnitude of the respective time constants of interstitials and vacancies. Good agreement is obtained with experimental data on irradiated materials for the main parameters of the interstitial loop populations. The present theory is also applied to the more complex conditions of void and bubble formation in irradiated materials. It is shown that the deviation of the helium bubbles in neu-tron-irradiated materials from their equilibrium conditions is primarily a result of the ratio of helium-to-displacement damage rates. Under the conditions of a low ratio (i.e. EBR-II), most helium bubbles can be regarded as voids. On the other hand, for higher ratios, helium bubbles are somewhat over-pressurized, particularly for small sizes.

Clustering of surface atoms during deposition processing of thin films is studied within the same framework. In this particular case,

the mobility of atomic clusters on the surface is sufficiently high, and a Fokker–Planck approximation is not applicable. Instead, we show that the moments of the distribution function can be obtained directly from the hierarchy of rate equations. Kinetic equations can be developed for the evolution of the moments, which completely describes both nucleation and growth of surface clusters. The basic difficulty in this application is shown to be the ability to reconstruct the distribution function from its moments. The method of maximum entropy is used, with additional constraints on the size distribution to obtain a unique, non-negative distribution function. The method is shown to be successful, when compared to exact analytical solution of a particular case. Eight to ten moments were shown to be sufficient, in the extreme case of a highly peaked distribution function.

An important feature of defect cluster formation in materials under non-equilibrium conditions is self-organization in regular spatial patterns. When space–time symmetry is broken, non-linear processes play a critical role in altering the microstructure. Under transient or pulsed irradiation conditions, the density of small interstitial clusters is greatly increased, while their size decreases, as compared to steady irradiation. On the other hand, at high enough temperatures, small vacancy clusters may actually dissolve during the off-time, and the net result is a much smaller amount of vacancy agglomeration into voids. It has been shown that pulsed irradiation at sufficiently high temperatures can lead to a smaller amount of swelling, as compared to steady irradiation.

Spatial fluctuations in the concentrations of point defects are shown to result in non-linear coupling with the relatively immobile features of the microstructure. Gradients, which develop in the concentrations of mobile point defects, result in self-organization of vacancy and interstitial defect clusters. One important ingredient which seems to be sufficient, even though not necessary, and which leads to spatial self-organization is the preferential production or absorption bias of freely migrating interstitials. The direct production of vacancy clusters in collision cascades, coupled with diffusion-reaction of mobile point defects lead to spatial instabilities. The emerging wavelength of the organized microstructure decreases with increasing dislocation network density, cascade collapse efficiency, and displacement damage rate. These predictions are in accord with experimental observations. It is also shown that a small degree of diffusion anisotropy of interstitial atoms

results in alignment of the organized microstructure along crystallographic directions, as observed experimentally.

Acknowledgments

The author would like to acknowledge the support of the Department of Energy, Office of Fusion Energy, for funding major parts of the reported research. The U.S. National Science Foundation funded work at UCLA on simultaneous clustering of point defects. NATO travel grants allowed collaboration with Prof. D. Walgraef (Free Univeristy of Brussels), with whom the work on instabilities was conducted. Funding from the German Government for post-doctoral research support for Dr. M. Vicanek to work on surface clustering is also acknowledged.

References

[1] M.V. Smoluchowski, *Z. Phys.*, **17** (1916) 557.
[2] M. Malek-Mansur and G. Nicolis, *J. Stat. Phys.*, **13** (1975) 197.
[3] I. Oppenheim, K.E. Schuler and G.H. Weiss, *Adv. Mol. Relaxation Processes*, **1** (1967) 13.
[4] N.M. Ghoniem, *Phys. Rev. B*, **39** (1989) 11810.
[5] N.M. Ghoniem and S. Sharafat, *J. Nucl. Mater.*, **92**(1) (1980) 121.
[6] U. Goesele, *J. Nucl. Mater.*, **78** (1978) 83.
[7] W.G. Wolfer and M. Ashkin, *J. Appl. Phys.*, **46** (1975) 547.
[8] N.M. Ghoniem and D.D. Cho, *Phys. Status Solidi (a)*, **54** (1979) 171.
[9] M. Kiritani, *J. Phys. Soc. Japan*, **35** (1973) 95.
[10] M.R. Hayns, *J. Nucl. Mater.*, **56** (1975) 267.
[11] W.G. Wolfer, L.K. Mansur and J.A. Sprague, in: *Proc. Intern. Conf. on Radiation Effects in Breeder Reactor Structural Materials*, (Eds.) M.L. Bleigerg and J.W. Bennet (Scottsdale, AZ, 1977) p. 841.
[12] J.A. Sprague, K.C. Russell and Y.H. Choi, Ref. [10] above, p. 1181.
[13] B.O. Hall, *J. Nucl. Mater.*, **91** (1980) 63.
[14] D.R. Olander, *Fundamental Aspects of Nuclear Reactor Fuel Elements* (NTIS, 1976) p. 215.
[15] N.M. Ghoniem and G.L. Kulcinski, *Radiation Effects*, **41** (1979) 81.
[16] N.Q. Lam, *J. Nucl. Mater.*, **56** (1975) 125.
[17] A.C. Damask and G. Dienes, *Phys. Rev.*, **120** (1960) 99.
[18] S. Chandrasekhar, *Rev. Mod. Phys.*, **15** (1943) 1.
[19] G.H. Weiss and M. Dishon, *J. Statist. Phys.*, **13** (1975) 145.
[20] R.I. Cukier, K. Lakatos-Lindenberg and K.E. Shuler, *J. Statist. Phys.*, **9** (1973) 137.
[21] H.R. Brager and J.L. Straalssund, *J. Nucl. Mater.*, **46** (1973) 134.
[22] T.M. Williams, *J. Nucl. Mater.*, **79** (1979) 28.
[23] P. Sigmund, *Phys. Rev.*, **184** (1969) 383.
[24] C.F. Clement and M.H. Wood, *Proc. R. Soc. London, Ser. A*, **368** (1979) 421.
[25] B.O. Hall and D.I. Potter, in: *Proc. 9th Intern. Symp. on Effects of Radiation on Structural Materials*, Richiand, WA, (1978) ASTM-STP-683, p. 789.
[26] J.L. Katz and H. Wiedersich, *J. Chem. Phys.*, **55** (1971) 753.